Plasmonic Force Propulsion Revolutionizes Nano/Picosatellite Capability

NASA Innovative Advanced Concepts
Phase I Final Report
Grant Number NNX13AP78G

May 29th, 2014

Principal Investigators
Joshua L. Rovey and Xiaodong Yang
Missouri University of Science and Technology
Rolla, Missouri 65409

Research Students
Paul D. Friz, Changyu Hu, Matthew S. Glascock

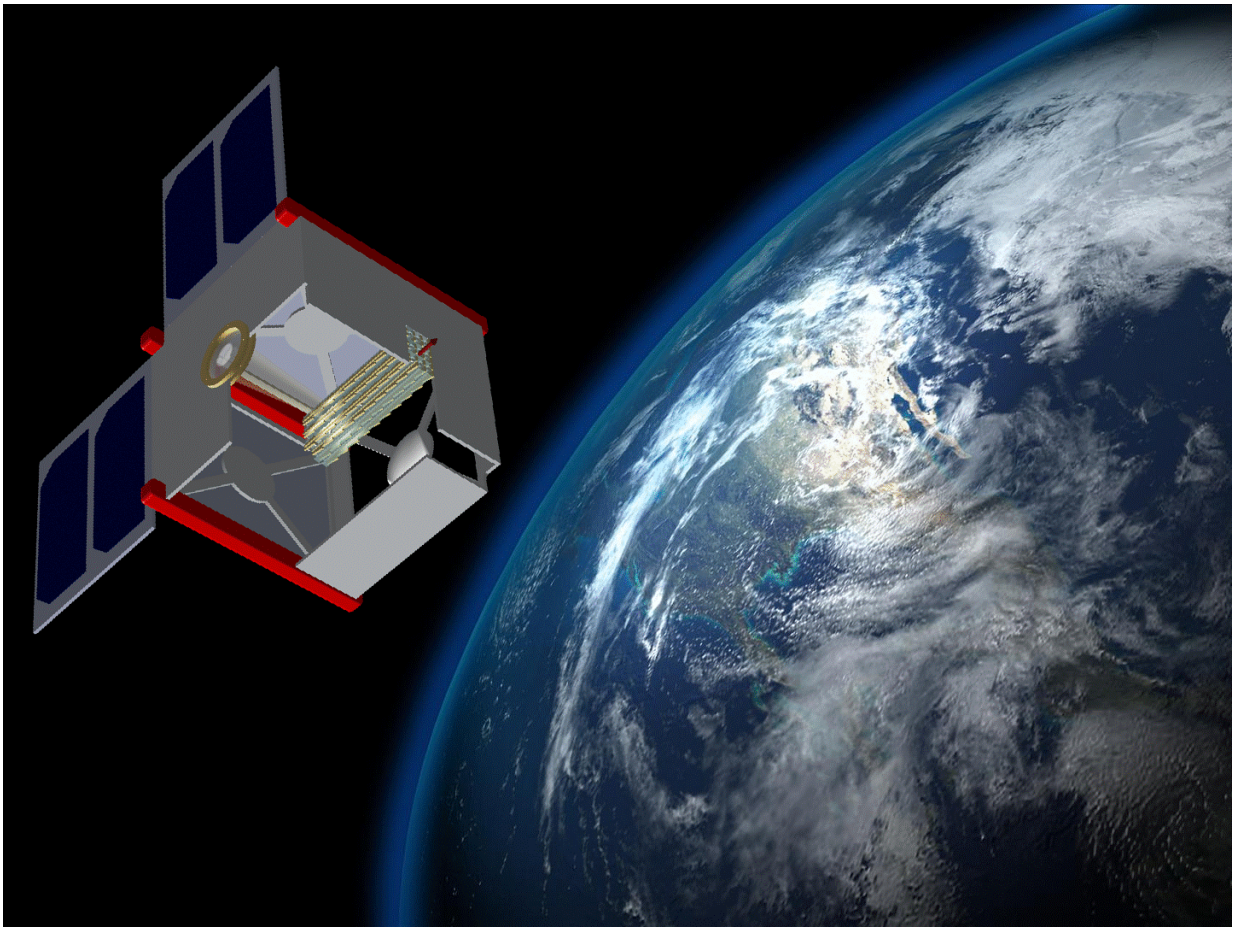

Executive Summary

This project investigated a new type of small spacecraft propulsion for attitude control, specifically proximity and precision pointing control. Plasmonic force propulsion uses solar light focused on deep-subwavelength nanostructures to excite strong optical forces that accelerate and expel nanoparticle propellant. The goal of the project was to assess the feasibility of plasmonic force propulsion for nano/pico-satellite applications by evaluating key mission parameters for a nano/pico-satellite using plasmonic force propulsion in a NASA-relevant mission context. We achieved this goal and objective by evaluating plasmonic force propulsion within a NASA mission that required attitude control and precision pointing of a small satellite. We numerically simulated plasmonic force fields with asymmetric/gradient geometry and relevant solar light constraints, predicted nanoparticle velocity, mass flow rate, and resulting propulsion performance (thrust, specific impulse), and evaluated spacecraft position control resolution and pointing precision. Additionally we compared the precision pointing capabilities of plasmonic propulsion, as well as the mass, volume, and power requirements, with other state-of-the-art control techniques, such as reaction wheels and colloid/electrospray electric propulsion.

The results are very exciting. Plasmonic force propulsion can significantly enhance the state-of-the-art in small spacecraft position and attitude control by 1-2 orders of magnitude. This is most succinctly shown in the figure below, which compares proximity and attitude control of plasmonic force propulsion (PFP) with other state-of-the-art thruster systems (μCAT, VAT, electrospray). Additionally this figure also shows the proximity and attitude control required for different existing (James Webb Space Telescope, Hubble) and future (LISA and Stellar Imager) NASA missions. While some of these NASA missions are not small spacecraft missions, the requirements serve to illustrate the fact that more precise proximity and attitude control will be required for future NASA science missions. Stellar imager is a proposed NASA missions that requires an extremely high pointing precision of 0.1 milliarcseconds (2.7×10^{-7} deg.) for an ultraviolet telescope that has over 200× the resolution of the Hubble Space Telescope, is able to take images showing details on the surfaces of other stars, consists of 20-30 small "mirror sats" flying in formation to produce a giant mirror, and requires each mirror-sat to be placed with nanometer precision and control its attitude with milliarcsecond precision.

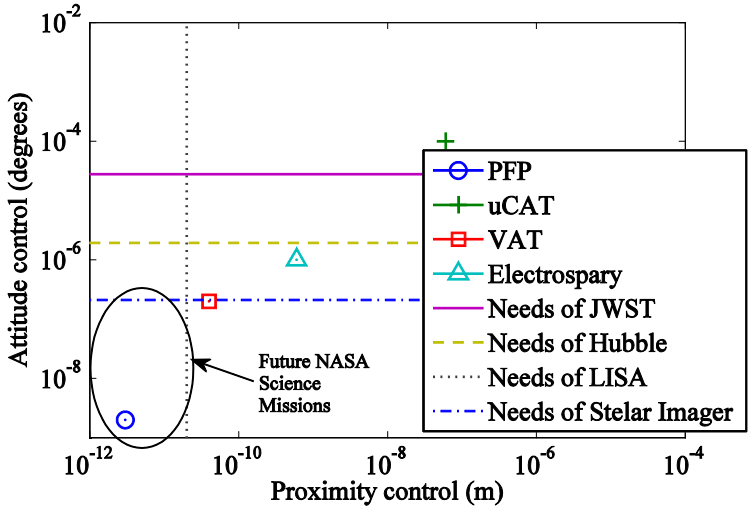

Our results have also elucidated the design geometry and configuration for a plasmonic force propulsion thruster, and we have created a conceptual design. A single plasmonic force propulsion thruster should consist of many individual asymmetric nanostructures arranged in a multi-stage, layered, array. Nanostructures should be arranged end-to-end in series to form a multi-stage because a single nanostructure produces very small force and multiple stages are necessary to achieve useable thrust and exit velocity. Multi-stage nanostructures should be layered (i.e., stacked) on top of each other. Each layer should be designed to resonate at a different wavelength within the broadband solar spectrum. This will maximize use of the broadband solar spectrum as shorter wavelength light is absorbed/resonates with top layers, while longer wavelength light passes through to resonate with lower layers. Finally, the multi-stage layers of nanostructures should be repeated in an array to provide increased thrust.

Results for a conceptual design of a plasmonic thruster that has 35 layers, 86 array columns, multi-stage length of 5 mm, a 5-cm-diameter light focusing lens, and uses 100 nm polystyrene nanoparticles expelled at a rate of $1x10^6$ per sec would have a thrust of 250 nN, specific impulse of 10 sec, and minimum impulse bit of 50 pN-s. The thruster mass and volume are estimated at 100 g and 50 cm^3, respectively. Comparison of dry mass and volume with other smallsat propulsion systems is shown in the figure below.

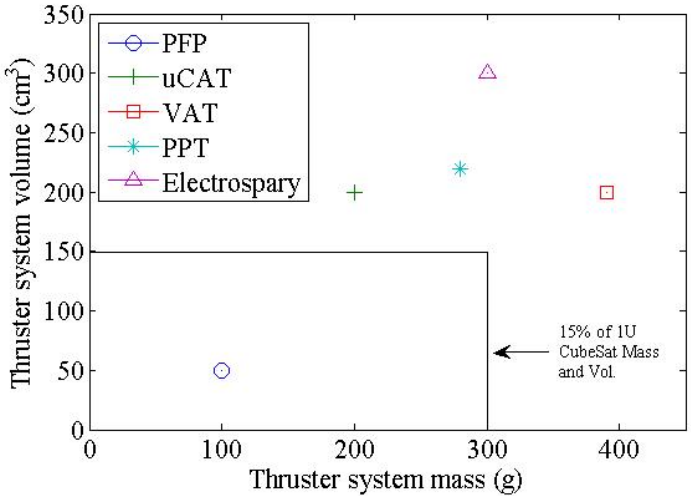

Plasmonic propulsion is ideally suited for proximity and attitude control maneuvers where the total spacecraft delta-V is relatively small (on the order of 1 m/s, compared with high delta-V orbit raising/maintenance maneuvers ~10-100 m/s). This is shown in the figure below. Because of its lower dry mass, plasmonic propulsion has a lower wet system mass for missions requiring delta-V of 3 m/s or less. This is ideal for proximity and attitude control where single maneuvers are mm/s, not main propulsion for orbit raising/maintenance.

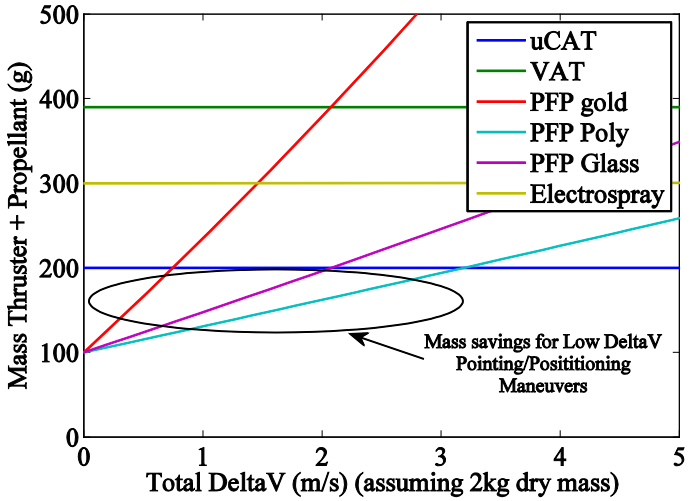

As a result of our study, the TRL of plasmonic force propulsion has been raised from 1 to 2. We have invented a practical application for the technology: space propulsion. This application is speculative, and our analytical and numerical studies presented here required assumptions without proof or detailed analysis. However, these studies show that plasmonic force propulsion has the potential to provide a 1-2 order of magnitude benefit in the precision pointing and proximity control for small spacecraft. Future efforts should focus on (1) further analyzing the concept within a mission context, (2) experimentally demonstrating nanoparticle acceleration with asymmetric nanostructures excited by the Solar spectrum, and (3) creating a roadmap for future development of supporting technologies. The combination of these future activities would raise the TRL to early 3.

The concept should be further analyzed within a mission context. An example specific nano/picosat mission should be determined and analyzed through detailed orbital dynamics calculations. This should include the effects of passing through Earth shadow, if necessary. A possible example mission might be the Stellar Imager, where nanometer level proximity control and 0.1 milliarcsecond pointing control are required between multiple nanosatellites.

Nanoparticle acceleration should be demonstrated experimentally using asymmetric nanostructures excited by the Solar spectrum. Individual asymmetric nanostructures relevant to plasmonic propulsion should be fabricated and characterized. Specifically the transmission spectrum of the nanostructure within the Solar spectrum should be characterized and compared with our numerical predictions reported here. Additionally, nanoparticle manipulation (acceleration) should be characterized and used to determine plasmonic force, which can then be compared with our numerical predictions reported here.

A roadmap should be created for future development of supporting technologies. Supporting technologies necessary for plasmonic propulsion have been investigated here, but a roadmap for future development is necessary. Important supporting technologies include large-scale nanostructure manufacturing, solar light distribution system (fiber optic) development, switching technology development (shutter, microblinds with electric glass), nanoparticle propellant reservoir and feed system development (high-pressure gas, plasmonic manipulation).

I. Introduction

A. The Concept

The concept is a plasmonic force propulsion system that will revolutionize the in-space maneuverability of small (nano, pico) satellites. The propulsion concept is built upon the growing field of plasmonics, which exploits the unique optical properties of metallic nanostructures to route and manipulate light at nanometer length scales. Plasmonic antennas and lenses can focus optical radiation into intense, engineered, localized field distributions or enable coupling to deep-subwavelength guided modes. Enhanced plasmonic forces enable manipulation and acceleration of nanoparticles, in what is commonly referred to as "optical tweezers."[1-3] In the proposed concept, illustrated in Figure 1, sun light is directly focused onto deep-subwavelength metallic nanostructures through a lens. The resonant interaction and coupling of the light with the nanostructure excites surface plasmon polaritons that generate a strong gradient optical force field. Nanoparticles (e.g., glass beads or metallic particles) are accelerated by the gradient force field and are expelled from the device at high speeds. Because the optical force field is coupled to the nanostructure through the strong light-matter interaction with surface plasmon polaritons, thrust is generated through momentum exchange with the expelled particles.

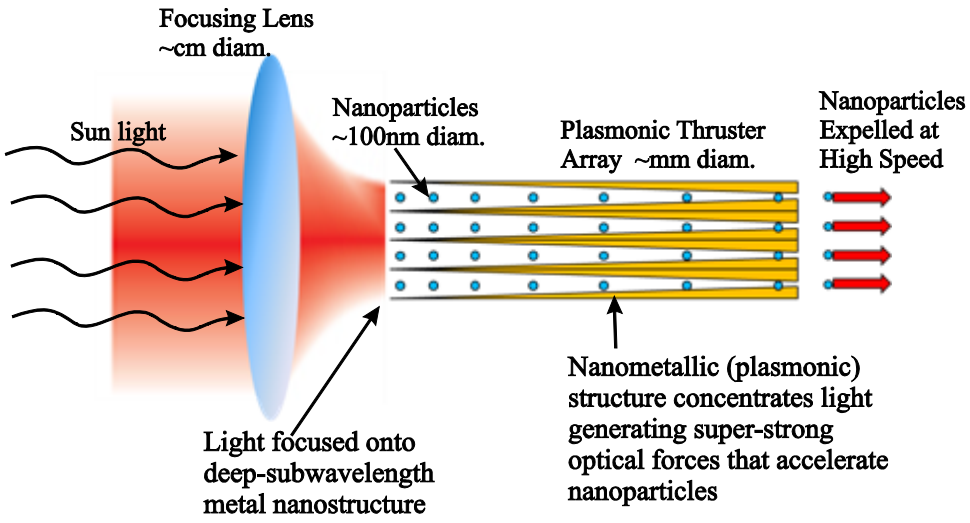

Figure 1: Schematic of proposed plasmonic force propulsion concept. Sunlight is focused onto a deep-subwavelength metallic nanostructure. The resonant interaction of the light with the nanostructure excites surface plasmon polaritons that generate a strong gradient optical force field. Nanoparticles are accelerated by the force field and expelled at high velocity. Nanoparticle acceleration is not due to photon pressure, but rather the strong gradient optical force field setup by surface plasmon polaritons excited by the strongly resonant light-matter interaction.

Careful examination of Figure 1 reveals a major benefit of the proposed concept: no electric or spacecraft power required. Solar energy is directly converted into propulsive thrust (jet power), additional solar cells, batteries, or other energy storage is not required. This has distinct advantages for the mass and power budget of a spacecraft, especially nano and picosats where mass and power are already severely limited. However, unlike other direct energy conversion

propulsion technologies (e.g, solar sails), plasmonic force propulsion is not due to photon pressure, but rather the strong gradient optical force field setup by surface plasmon polaritons excited in the designed metallic nanostructures by the strongly resonant light-matter interaction. This has distinct advantages in terms of the physical size, mass, and performance of the propulsion system, details of which are provided below.

B. Motivation

The full potential of small spacecraft remains untapped because they lack maneuverability. Plasmonic force propulsion provides attitude control capability for small spacecraft with no power penalty and minimal mass and volume penalty. This creates new capabilities for small spacecraft enabling NASA science and exploration missions that were previously impossible. Examples of new capabilities of small spacecraft include precise orientation for imaging, sample collection, and/or data collection, alignment of spacecraft clusters/formations, orbit adjustment/control around asymmetric bodies (e.g., asteroids), at Lagrange points, and at inter-space staging locations.

One of NASA's strategic goals is expanding scientific understanding of the Earth and the universe [4]. One specific mission related to that goal and enabled by the concept is detailed asteroid mapping. A small satellite (e.g., cubesat) deployed from a mother satellite could use its plasmonic force propulsion system to orbit the asteroid investigating its 3D shape, composition, rotation, etc., information that can elucidate the early solar system and potential for asteroid mining. Another NASA goal is to identify and investigate exoplanets, planets outside our solar system [4]. The measurements necessary to study exoplanets are quite challenging and require extremely sensitive instruments that must be precisely pointed at the region of interest. The Astrophysics Strategic Mission Concept Studies most stringent requirement is 0.1 milliarcseconds for the ACCESS mission [5], which is 50 times more precise than the state-of-the-art 5 milliarcseconds for Hubble. The proposed plasmonic propulsion concept can enable and enhance these types of missions by providing very small thrust and impulse bits to precisely orient a spacecraft or align a constellation of satellites.

Plasmonic force propulsion is exciting because it has the potential to solve the major challenge for small spacecraft: propulsion. This advancement would provide a giant leap in small spacecraft capabilities by enabling maneuverability. Further, it has the potential to impact the fast-growing and already large market of small satellite designers and manufacturers, ranging from large industrial entities to small university student groups. What's more, plasmonic force propulsion has minimal power, mass, and volume requirements and could therefore be easily integrated into existing small spacecraft architecture.

The major challenge for small spacecraft remains propulsion. Micci and Ketsdever [6] compiled micropropulsion state-of-the-art in 2000. And many of those micropropulsion systems are highlighted by NASA in its technology roadmap [7] (e.g., microresistojets, microcavity discharge thrusters, mini ion/Hall, pulsed plasma thrusters, and electrospray MEMS). New concepts have also been investigated (e.g., nanoparticle field extraction, laser ablation, free molecule resistojet). While significant advances have been made, small spacecraft still lack propulsion for the same reasons outlined by Micci and Ketsdever [6]: mass, power, and volume constraints.

Plasmonic force propulsion of spacecraft has not been explored. However, nanoparticle manipulation using strong optical forces generated by surface plasmon polaritons is well-known technology within the plasmonics community. Previous research has demonstrated trapping and propulsion of nanoparticles in 2D geometries within aqueous and air environments [8-10]. Plasmonics is a flourishing new field of science and technology offering unusual optical capabilities and a tantalizing opportunity to attain unprecedented levels of synergy between optical and electronic functions. Nanometallic objects derive their optical properties from an ability to support collective electron oscillations, known as surface plasmons. At present, plasmonics research enables new fundamental science and device technologies, and there is a dramatic growth in both the number and scope of plasmonic applications.

There are four main characteristics that need to be explored to better evaluate this technology: 3D geometry, asymmetric/gradient geometry, vacuum operation, and zero-g operation. Previous studies have used 2D symmetric geometry in aqueous and air environments in gravity. Application of the technology to space propulsion will require that similar phenomena are present and similar or even enhanced results (significant nanoparticle acceleration) can be achieved with those characteristics. This concept will break new ground because it will be the first investigation of plasmonic forces generated directly from sun light to control small satellites with high precision. Further, it will contribute to new understanding of the approach by investigating new gradient geometries, while also studying the resonance spectra of plasmonic nanostructures. Optical trapping based on plasmonic force has been studied before, but here we investigate the gradient plasmonic force based on the tapered metallic nanostructures in order to provide thrust from particle acceleration. Our study provides a new concept to manipulate and drive nanoparticles with enhanced plasmonic force generated from tapered metallic nanostructures excited by sun light.

C. Goal, Objectives, and Approach of the Study

The **goal** of our study is to assess the feasibility of plasmonic force propulsion for nano/pico-satellite applications. Our **objective** is to evaluate key mission parameters for a nano/pico-satellite using plasmonic force propulsion in a NASA-relevant mission context. The NASA-relevant mission context we will evaluate the concept within is attitude control and precision pointing of a small satellite. In order to assess the thruster concept within this context, we must have a prediction of the anticipated propulsion performance. An overview of our approach is shown in Figure 2. Our **approach** is to use numerical and analytical modeling to predict plasmonic thruster propulsion performance and then use that information as an input to evaluate key attitude control and precision pointing parameters. Our **specific objectives** are to (1) numerically simulate plasmonic force fields with asymmetric/gradient geometry and relevant solar light constraints, (2) predict nanoparticle velocity, mass flow rate, and resulting propulsion performance (thrust, specific impulse), and (3) evaluate spacecraft position control resolution and pointing precision. Additionally we plan to compare the precision pointing capabilities of the proposed technology, as well as the mass, volume, and power requirements, with other state-of-the-art control techniques, such as reaction wheels and colloid electric propulsion.

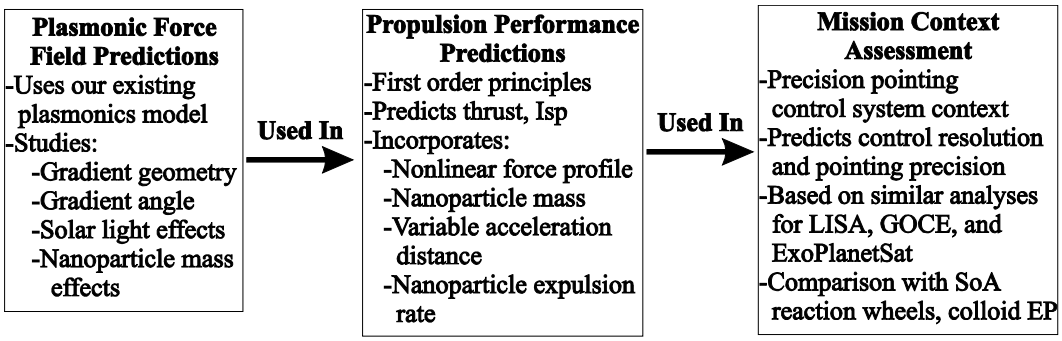

Figure 2: Overview of our approach to assess plasmonic force propulsion within a small-satellite precision pointing mission context.

II. Results of the Study

In the following sections we present results from numerical simulations of plasmonic force fields, propulsion performance predictions, and mission context assessment. Additionally we present the conceptual design of a plasmonic force propulsion thruster and also explore and answer other questions regarding the concept.

A. Specific Objective 1: Numerical Simulations of Plasmonic Force Fields

We investigated the plasmonic force field produced by a three-dimensional nanoscale structure that is designed to produce a gradient optical force. A gradient optical force is necessary to expel nanoparticle out of the nanostructures rather than trap them within the nanostructure. First we describe the numerical model used to predict plasmonic force fields and nanostructure transmissions spectra, then we present the different nanostructures investigated followed by the results and conclusions.

1. Numerical Model

The momentum of light has been a fascinating research area for many years. Even today, the true nature of the photon's momentum raises a lot attention. This momentum is normally too small to have any significant effect, but in nanoscale structures the transfer of linear momentum between light and matter and the associated optical force have been widely studied. Generally, these forces can be divided into scattering and gradient forces, depending on whether the transferred momentum is parallel or perpendicular to the direction of propagation. Optical scattering forces can be used to cool atoms through the interaction with intense laser light. Optical gradient forces are used in optical tweezers, where microscopic dielectric particles are trapped and moved by laser beams towards regions of highest intensity. Recently, optical gradient forces have been investigated in various plasmonic nanostructures, for example, gold nanoparticle dimers and coupled metal planar waveguides. On the basis of plasmonic nanostructures with sub-wavelength mode volume, nanoscale optical tweezers with trapping volume beyond the diffraction limit can also be realized for optical trapping of a single nanoparticle. Besides, surface plasmon polaritons (SPPs) confine the electromagnetic waves into a deep sub-wavelength scale. Such a strong optical confinement results in significantly enhanced optical field strength and gradient of light field. In this case the optical gradient force will be greatly enhanced. In the following content, optical gradient forces have been studied to move and accelerate the nanoparticle in plasmonic nanostructures.

We report a realization of three-dimensional nano-metric asymmetry trapezoid structures based on nanostructured substrates to enhance the gradient optical force and propel the nanoparticle out of the nanostructures. The strong coupling between the nanostructures SPP mode is supported at the interface of the nanostructures and the nanoparticle. The finite-element analysis method (FEM) is used to calculate the optical force of the nanostructure. A screenshot from the COMSOL multiphysics suite used to perform the calculation is shown in Figure 3. The asymmetry gold trapezoid structure is designed to generate the giant optical force, which is stimulated by the solar radiation to move nanoparticles. The nano-scale fabrication durable geometry structure is fixed to get the strongest coupling optical force in solar light wavelength range, based on the TM polarization of the incident light (where the electric field is vertical) and the confined air gap.

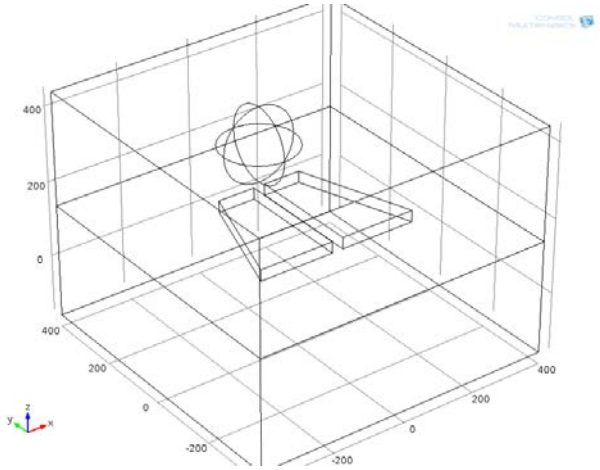

Figure 3: Schematic of nanoscale asymmetry trapezoid structures in 3D. And silicon nanoparticles are subjected to the gradient optical force and pushed out of the nanostructures

The coupling strength determines the optical energy concentration in the gap region, and is related to the gradient optical force generated on the gold nanostructures. This can be calculated by integrating the Maxwell's stress tensor around any arbitrary surface enclosing the nanostructures. The total gradient optical force on the charges in nanoparticle volume V:

$$\boldsymbol{F} = \int_v (\boldsymbol{E} + v \times \boldsymbol{B})\rho d\tau = \int_v (\rho \boldsymbol{E} + \boldsymbol{J} \times \boldsymbol{B}) d\tau \quad (1)$$

The force per unit volume is

$$f = \rho \boldsymbol{E} + \boldsymbol{J} \times \boldsymbol{B} \quad (2)$$

eliminating ρ and **J** by using Maxwell's equations:

$$f = \epsilon_0 (\boldsymbol{\nabla} \cdot \boldsymbol{E})\boldsymbol{E} + (\frac{1}{\mu_0}\boldsymbol{\nabla} \times \boldsymbol{B} - \epsilon_0 \frac{\partial \boldsymbol{E}}{\partial t}) \times \boldsymbol{B} \quad (3)$$

Now

$$\frac{\partial}{\partial t}(\boldsymbol{E} \times \boldsymbol{B}) = \left(\frac{\partial \boldsymbol{E}}{\partial t} \times \boldsymbol{B}\right) + (\boldsymbol{E} \times \frac{\partial \boldsymbol{B}}{\partial t}) \quad (4)$$

According to Faraday's laws

$$\frac{\partial \boldsymbol{B}}{\partial t} = -\boldsymbol{\nabla} \times \boldsymbol{E} \quad (5)$$

So

$$\frac{\partial \boldsymbol{E}}{\partial t} \times \boldsymbol{B} = \frac{\partial}{\partial t}(\boldsymbol{E} \times \boldsymbol{B}) + \boldsymbol{E} \times (\boldsymbol{\nabla} \times \boldsymbol{E}) \quad (6)$$

Thus

$$f = \epsilon_0[(\boldsymbol{\nabla}\cdot\boldsymbol{E})\boldsymbol{E} - \boldsymbol{E}\times(\boldsymbol{\nabla}\times\boldsymbol{E})] + \frac{1}{\mu_0}\left[\mathbf{B}\times(\boldsymbol{\nabla}\times\boldsymbol{B}) - \epsilon_0\frac{\partial}{\partial t}(\boldsymbol{E}\times\boldsymbol{B})\right] \quad (7)$$

And it can be simplified into the Maxwell stress tensor.

$$T_{ij} \equiv \epsilon_0\left(E_iE_j - \frac{1}{2}\delta_{ij}E^2\right) + \frac{1}{\mu_0}\left(B_iB_j - \frac{1}{2}\delta_{ij}B^2\right) \quad (8)$$

The indices i and j refer to the coordinates *x*, *y* and *z*. The stress tensor has a total of nine components (T_{xx}, T_{yy}, T_{xz}, T_{yx}, and so on). δ_{ij} is the Kronecker delta. According to Eq. 8, optical gradient force is calculated based on trapezoid nanostructures subjected to Solar light spectrum from 400nm to 1100nm. Specific nanostructures have been analyzed within the Solar spectrum and are described in the following section.

2. Nanostructure Geometry Investigated

Figure 4 shows the schematic of trapezoid structures in 2D views. This asymmetric nanostructure is designed to generate gradient optical electric field in the presence of light within the 400-1100nm band of Solar light. The finite-element analysis method (FEM) is used to calculate the optical force of the nanostructure on the nanoparticle, using the Eq.8. In Figure 4, the incident light is transverse magnetic (TM-) polarization of the incident light (where the electric field is along X-axis). The radius of the glass (Silicon Dioxide) nanoparticle is 100nm and is 10nm above the surface of the nanostructure. The different nanostructures investigated are shown in Figure 4. All investigated nanostructures are assumed to be gold (Au) nano-trapezoids with a length of 400 nm. Due to the asymmetric structure, the nanoparticle experiences an optical force that is dependent on its position along the Y-axis and move towards the other side of the nanostructure, as shown in Figure 4. The incident light has the TM polarization where the electric field is horizontal along the X-axis. For the desired resonance wavelength, the width of the structures can be tuned so that the strongest optical field concentration inside the metallic structure will be realized. By having nanostructures with different geometry parameters, full solar spectrum from 400 nm to 1100 nm can be covered.

Figure 5(a) shows the schematics of asymmetric metallic nanostructures with different geometry parameters. As the width decreases, the nanostructure will support lower resonance wavelength. As one example, Figure 5(b) plots the electric field intensity distributions of asymmetric nanostructure with the width of 100 nm at the resonance wavelengths of 800 nm based on our numerical simulation results. Both the 3D view and 2D view are shown in the figure. It is clear that the optical field maximum is located close to the structure end with large width so that the nanoparticle will be pushed from the end with small width to the other end with large width along the Y-axis. Nanostructures with other geometry parameters supporting different resonance wavelengths will have the similar optical field distributions.

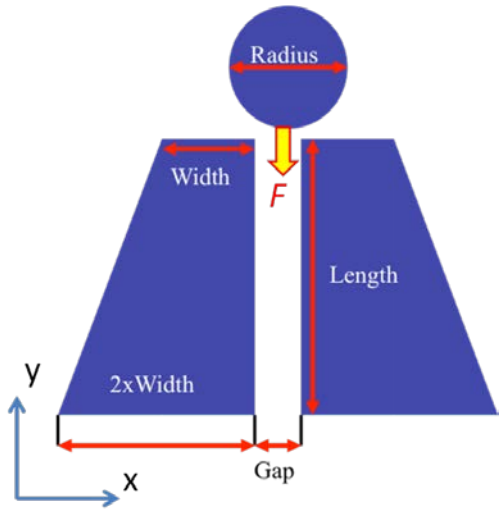

Figure 4: Schematic of nanoscale asymmetry trapezoid structures in 2D views. The incident light will excite the optical resonance of the nanostructure so that gradient optical force will be generated on the nanoparticle and thus the nanoparticle will be accelerated along the negative Y-axis. The arrow shows the direction of the nanoparticle movement.

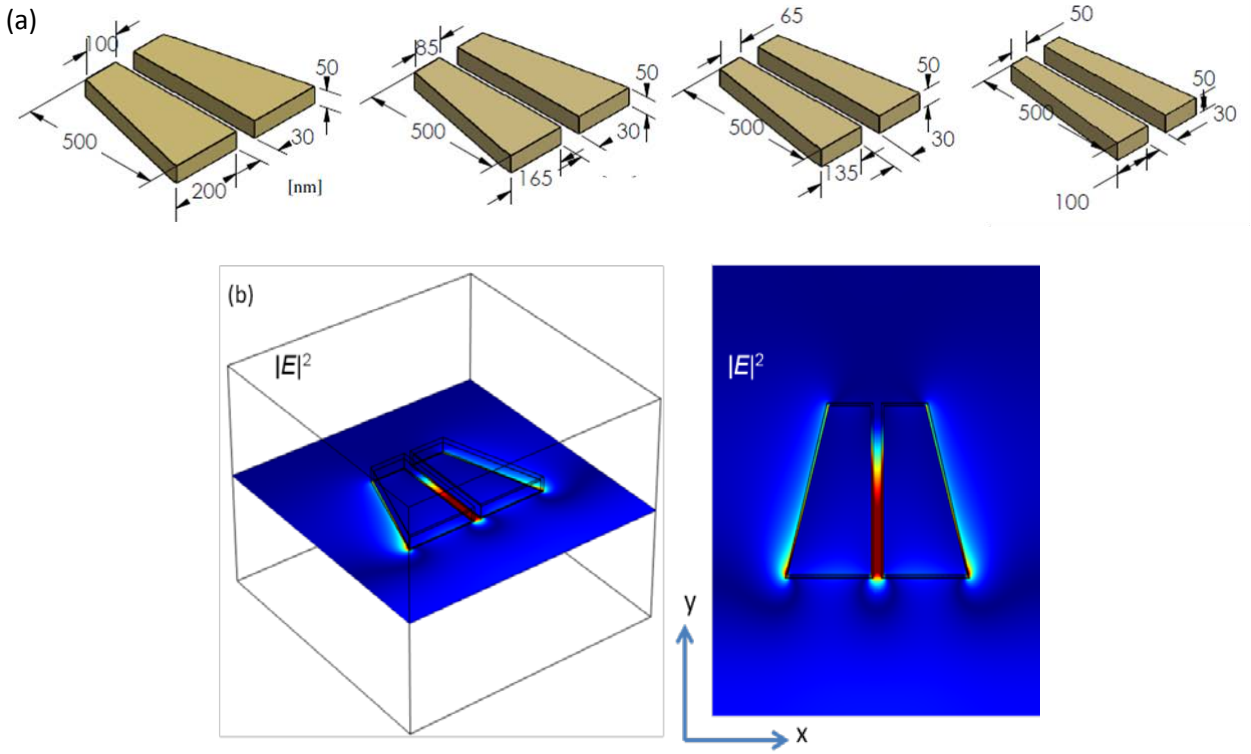

Figure 5: (a) Schematics of asymmetric metallic nanostructures with different geometry parameters. As the width decreases, the nanostructure can support lower resonance wavelength. (b) Asymmetric nanostructures we have investigated with numerical simulations. The electric field intensity distributions of asymmetric nanostructure with the width of 100 nm at the resonance wavelength of 800 nm are shown. Both the 3D view and 2D view are shown in the figure.

3. Transmission Spectra and Force Field Results

Transmission spectrums for the investigated nanostructures are shown in Figure 6. Each nanostructure exhibits a strong resonance within a narrow band (~20 nm) of the Solar spectrum (Figure 7a). Because of the different dimensions of the nanostructures, each nanostructure resonates at a different wavelength. The four nanostructures investigated have strong resonance at 400 nm, 500 nm, 800 nm, and 1100 nm in the solar spectrum. The result shows the strong optical resonance from the nano-trapezoid with expected wavelength position, and implies the giant gradient electric field generated within those kinds of nanostructures. The strong optical resonance in the transmission spectrum indicates the strong light confinement and absorption properties. By using nanostructures with different geometry sizes, broadband solar light from 400 nm to 1100 nm can be fully used to create strong optical field resonance and therefore gradient optical forces.

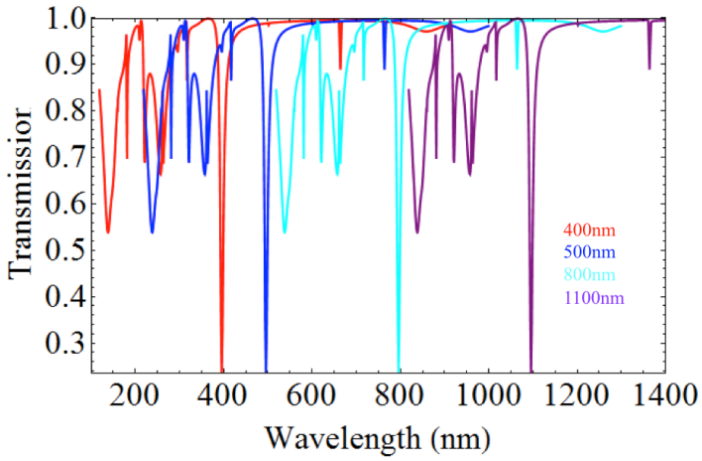

Figure 6: Transmission spectrums of investigated nanostructures in solar light wavelength range from 400 nm to 1100 nm.

Resonance wavelength (nm)	Width (nm)	Gap (nm)	Length (nm)
400	40	50	50
500	50	30	30
800	100	30	30
1100	150	30	30

Table 1: Different geometry parameters of trapezoid nanostructures for realizing various resonance wavelengths within the soalr spectrum from 400 nm to 1100 nm. The width of the trapezoid structures is increased to reach longer resonance wavelength. The length of the trapezoid structures will be kept as 400 nm.

Different geometry parameters of trapezoid structures can influence the position of optical resonance wavelength. The width and gap of the nanostructure (as shown in Figure 4) can be used to tune the optical resonance into different wavelengths within the solar light spectrum. The specific dimensions of the investigated nanostructures and their resonant wavelength is listed in Table 1. Resonant wavelength increases from 400 nm, 500 nm, 800 nm, 1100 nm as the width of the trapezoid structures increases from 40nm to 150nm, while the length is kept as 400 nm. The

gap size can be tuned from 30 nm to 50 nm and it has almost no influence to the resonance wavelength of the nanostructure.

Figure 7a shows the solar spectrum. The optical force on the nanoparticle as a function of its position along the Y-axis was calculated using Eq. 8 and the results are shown in Figure 7b. The position Y=0 nm corresponds to the center of the nanoparticle at the end of the nanostructure with the narrow width. The particle experiences a positive force that increases to a maximum at the other end of the nanostructure (the widest end) and then decreases as the nanoparticle moves away out from the nanostructure. At the location of approximately 800 nm out from the nanostructure, the nanoparticle experiences negative optical force which means that the nanoparticle will be slightly decelerated but will still move towards outside. Since the net optical force over the entire length (from 0 to 1500 nm) is positive, the nanoparticle will move along one direction and eventually be expelled outside from the nanostructure.

The force profile (F(y)) for each investigated nanostructure is different because of the different resonant wavelength. The broadband solar spectrum has an irradiance of ~1.85 W/m^2 at 500 nm, and decreases to ~1 W/m^2 at 800 nm. As the incident solar power decreases, the optical force exerted on the nanoparticle also decreases. Each of the nanostructures investigated will receive a different intensity of light based on where its respective resonance wavelength is located in the solar spectrum. The largest optical force, which occurs at the end of the trapezoid structure, increases from 20 pN/W to 65 pN/W as the nanostructure resonant wavelength decreases from 1100 to 500nm. While the largest optical force decreases from 65 pN/W to 45 pN/W as the resonant wavelength decreases from 500 to 400 nm. Again, these optical force trends are due to the relative optical intensity across the solar spectrum showing a blackbody emission from the Sun with the peak optical intensity at ~500 nm (Figure 7a). The result shows that the optical gradient force can accelerate the nanoparticle along Y-axis in nano-trapezoid structure, and is a promising technology to be harnessed for the propulsion of nano-satellites.

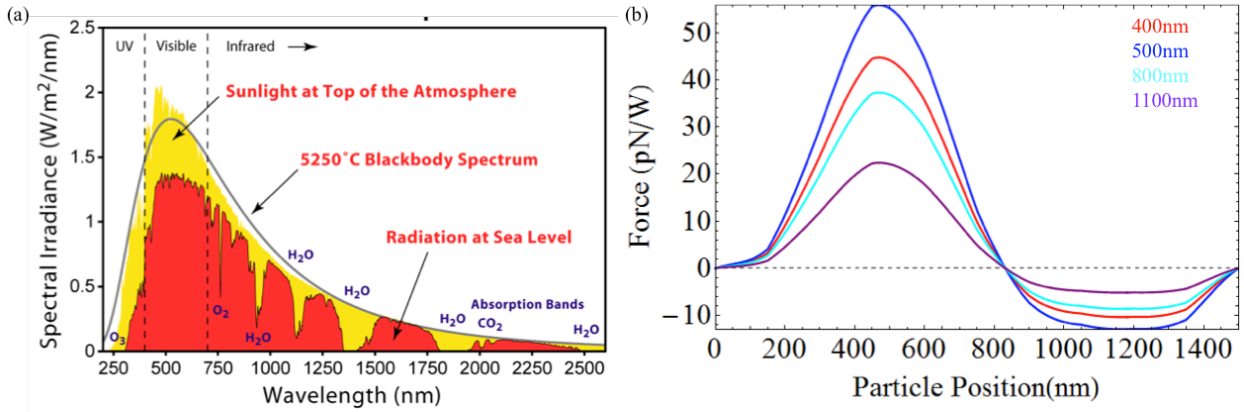

Figure 7: (a) Solar radiation spectrum; (b) The calculated optical forces exerted on the nanoparticle at different resonance wavelength of 400, 500, 800, and 1100 nm within the solar spectrum.

4. Main Conclusions

Nanostructures can be designed to produce gradient optical forces that will accelerate and expel nanoparticles. Further, the nanostructures can be designed to resonate strongly at wavelengths

within the solar spectrum. The resonant light-matter interaction in the nanostructure will generate optical forces of tens of pN/W which can be used for propulsion applications. Our initial concern regarding the compatibility of broad band solar light spectrum with the narrow resonance band of plasmonic nanostructures was not found to be a problem. In fact, not only can asymmetric nanostructures resonate within the solar spectrum, but they have quite narrow resonance band (~20 nm) which is advantageous for developing compact multilayered arrays of nanostructures with different resonance wavelength covering the whole solar spectrum in order to maximize the use of solar light (this topic further discussed in the following section) to create as large force as possible. The biggest challenge is the small forces imparted on nanoparticles. With incident power on 1 nanostructure expected to be ~1-2mW, the maximum force on the nanoparticle is only 0.1 pN. It is clear from the plasmonic simulations that a multi-stage geometry is required to achieve acceleration necessary for propulsion (multiple nanostructures need to be placed in series with each other). Further, because of the narrow resonance band it is possible to layer or stack nanostructures on top of each other, thereby maximizing use of the solar broadband, minimizing cross-sectional area, and maximizing solar intensity. Because the nanostructures absorb/resonate at a very narrow band, off-resonant wavelengths are not absorbed and pass readily through lower layers within the stack.

B. Specific Objective 2: Plasmonic Propulsion Performance Predictions

We predicted plasmonic thruster propulsion performance. Nanostructure force profiles obtained from specific objective 1 were used in an analytical propulsion performance model to predict the thrust and specific impulse of a plasmonic force thruster. Specifically, results from specific objective 1 were used to develop a conceptual plasmonic force thruster. The impact of important thruster design variables, such as nanoparticle size and mass, nanoparticle exhaust rate, nanostructure array size, and incident power, were studied.

1. Conceptual Design of a Plasmonic Propulsion Thruster

The general conceptual design of a plasmonic propulsion thruster, based on the knowledge gained from nanostructure simulations (specific objective 1), is shown in Figure 8. It is a layered multi-stage array of nanostructures. Multiple nanostructures must be placed end-to-end (in series, a multi-stage geometry) in order to provide an appreciable acceleration of the nanoparticle propellant. This is the multi-stage length, and also the acceleration length, L. A layered structure is beneficial for efficient use of solar light. Nanostructures on top resonate with shorter wavelengths of the solar spectrum, while the longer wavelengths pass through to resonate with deeper layers. A structure with 4 layers is shown in the figure below, but transmission spectra results (Figure 6) show that the absorption/resonant band is very narrow for a particular nanostructure. This means that many more layers can be used and the following analysis assumes 36 layers each with a 20 nm resonance band within the 400-1100 nm solar broadband. In between each layer is a nanoparticle guide tube. Nanoparticle propellant is accelerated and expelled from the guide tube by plasmonic forces applied from the nanostructure layers directly above and below it. The following analysis assumes there are 36 layers of nanostructures with 35 guide tube in between. This layered multi-stage structure is repeated (columns) to form a large array of N elements, where N = layers (rows) x columns. The area solar light is incident upon is the thruster area, $A_{thruster}$, and is the acceleration length, L, times the number of columns in the array. Not shown in the figure below is the solar light focusing lens.

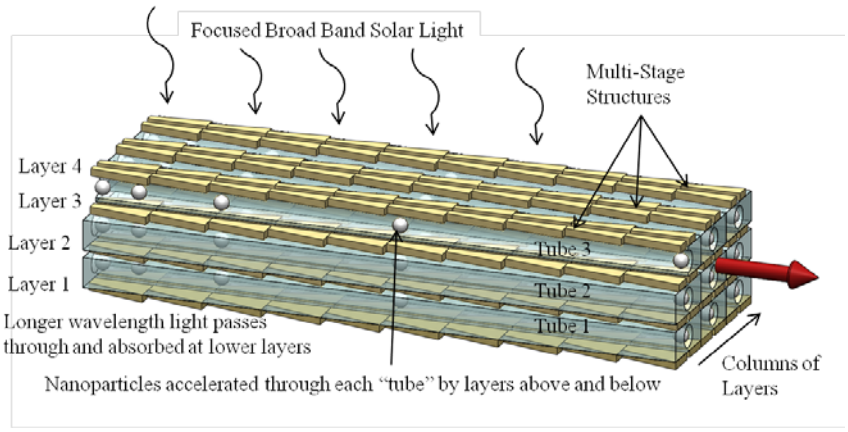

Figure 8: Illustration of a plasmonic force thruster. Incident focused broad band solar light resonates with each layer of nanostructures. Longer wavelengths are absorbed (resonate) with deeper layers. In between each nanostructure layer are nanoparticle guide tubes. Nanoparticle propellant is accelerated and expelled from the guide tube by the combination of forces from the nanostructure layers above and below it.

2. Analytical Propulsion Performance Model

The performance of a plasmonic thruster was analytically modeled based on the design parameters of the conceptual model shown in Figure 8. Specifically, both thrust and specific impulse are predicted using fundamental physics models. Solar light power incident on the thruster is dependent on the focusing lens diameter (area, A_{lens}) as shown in Eqn. 9, where I is solar intensity in low-Earth orbit (1.4 kW/m^2). The solar light power incident on a single nanostructure that makes up the thruster array is given by Eqn. 10. It is clear from this relationship that maximizing the collection lens size and minimizing the thruster area increases the power incident on each individual nanostructure, which increases the accelerating plasmonic force on the nanoparticle propellant (Figure 7b).

$$P_{thruster} = IA_{lens} \tag{9}$$

$$P_{nanostructure} = P_{thruster}\frac{A_{nanostructure}}{A_{thruster}} = I\frac{A_{lens}A_{nanostructure}}{A_{thruster}} \tag{10}$$

Incident solar light excites surface plasmon polaritons in each nanostructure of the thruster array, resulting in an optical force on the nanoparticle propellant as given by Figure 7b. The force is a function of position within each individual nanostructure, and is therefore a function of position along the entire multi-stage series of nanostructures, F(y). The force profile for an individual nanostructure is given by the results of the electrodynamic simulations shown in Figure 7b. This single nanostructure force profile is assumed to be the same for each nanostructure constituting the entire multi-stage assembly of nanostructures. Additionally, the force profile is different for each layer of the multi-stage geometry. That is, each layer has a nanostructure with different dimensions to resonant with a different desired bandwidth of the solar spectrum, and, as a result of the relative intensity across the solar spectrum and the efficiency of different nanostructure geometry, the force profile is different for each layer, as shown in Figure 7b. For example, at 500 nm, the solar broadband has an intensity of ~1.85 W/m^2, whereas at 800 nm, it is ~1.14 W/m^2. We extrapolate the results for all 36 layers based on the results from the four nanostructures

simulated above, results shown in Figure 7b. The extrapolated results across all 36 layers are shown in Figure 9.

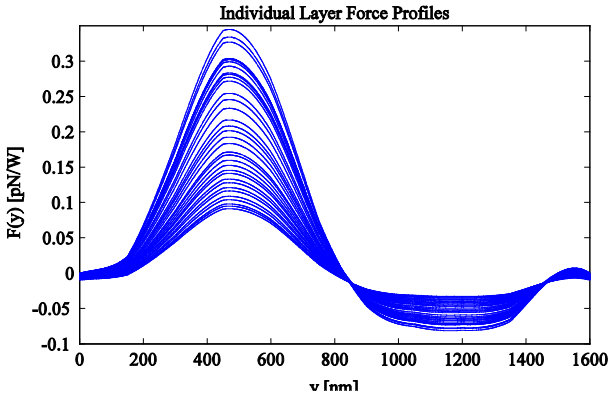

Figure 9: Optical (plasmonic) force applied to a 100 nm nanoparticle for each of the 36 layers of the conceptual plasmonic thrusters.

The final velocity of the nanoparticle propellant is calculated using Eqn. 11, where v_i is the final velocity (assuming zero initial velocity) of the nanoparticle out of tube i, $F_{above,below}(y)$ is the force profile associated with the multi-stage nanostructure layer above or below the nanoparticle guide tube, L is the length of the multi-stage nanostructure, and m is the mass of the nanoparticle. Each layer of the thruster is expelling nanoparticles at different velocity because the plasmonic force on the nanoparticle is different for each nanostructure geometry. The distribution of nanoparticle velocity across the exitplane of the thruster is shown in Figure 10. Notice that the nanoparticle velocity is the same for each layer (horizontal direction in figure), but is different for different layers (vertical direction in figure).

$$\frac{v_i^2}{2} = \int_0^L \frac{F_{above}(y) + F_{below}(y)}{m} dy \tag{11}$$

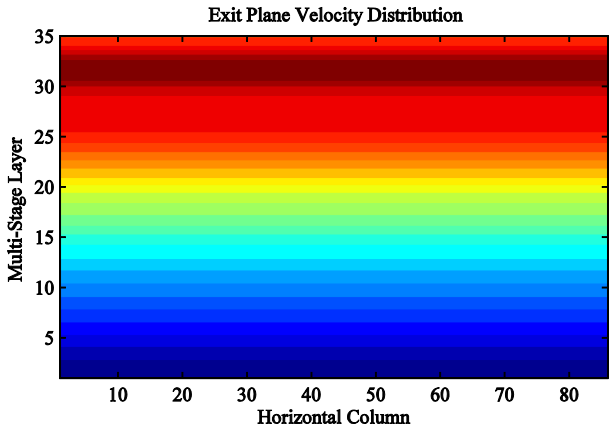

Figure 10: Velocity distribution over the thruster device exit plane cross section for the conceptual thruster design of 35 layers and 86 array columns.

The total thrust force (T) of the thruster array is the sum of the thrust produced by each individual tube expelling nanoparticles. Each layer is expelling nanoparticles at different velocity, but the model assumes each tube is expelling nanoparticles with the same mass, m, and at the same rate, f. The thrust can be calculated using Eq. 12 below, where N is the number of guide tubes in the array (the size of the array) and f is the rate at which the nanoparticles are being expelled from each tube (sec^{-1}). Specific impulse (I_{sp}) is calculated using Eqn. 13, where $g_0 = 9.81$ m/s^2.

$$T = \sum_{i}^{N} \dot{m} v_i = \sum_{i}^{N} m f v_i \tag{12}$$

$$I_{sp} = \frac{T}{\dot{m} g_0} = \frac{T}{N m f g_0} \tag{13}$$

3. Propulsion Performance Results

The following sections describe results from the propulsion performance model. Specifically, the effects of particle mass (size and density, $m = \rho V$), acceleration length, L, expulsion rate, f, array size, N, and collection lens size, A_{lens}, on propulsion performance (T, I_{sp}) are investigated.

Preliminary analysis using representative force profile data offers a good basis to determine how the key performance characteristics will depend on the constraints of the plasmonic simulations, as well as characteristics of the nanoparticle. Thrust force and specific impulse directly depend on the mass, and thus implicitly the density and size of the nanoparticle being expelled. Gold, glass, and polystyrene nanoparticles are investigated because these are commonly used in nano-optics and plasmonic experiments. Figure 11 below shows representations of each of these nanoparticles, as well as a comparison of nanoparticle mass relative to size (diameter) of the particles.

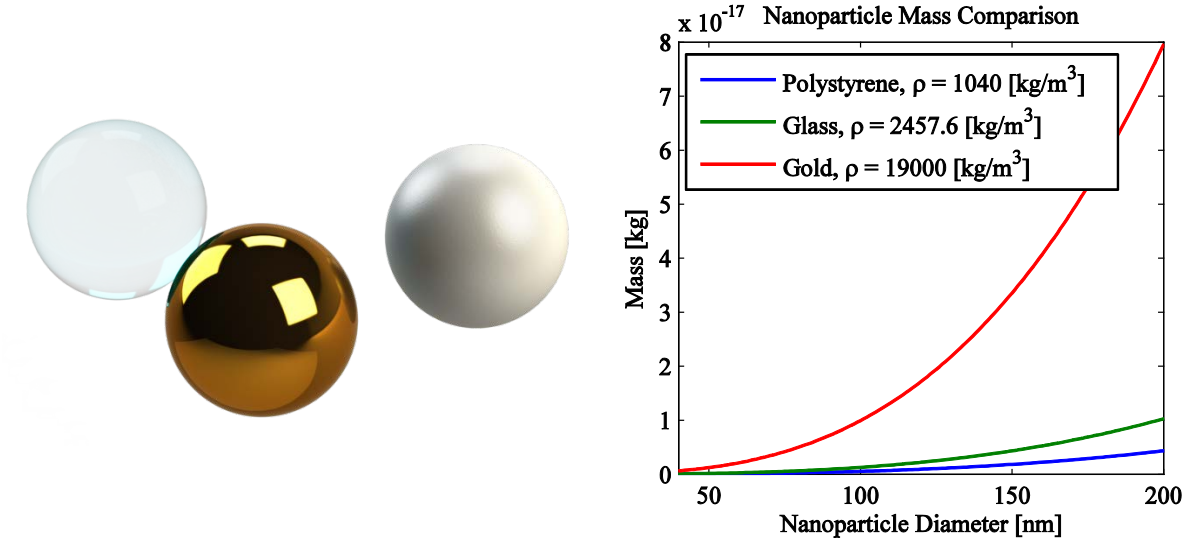

(a) (b)

Figure 11: Possible nanoparticle propellants. (a) Representative images of the particles. (b) Comparison of the masses of the proposed particles with variation in particle diameter.

The effect of nanoparticle type and size on propulsion performance is shown in Figure 12. The analysis assumes a 5 mm acceleration length (L), particle expulsion rate (f) of 1x10^6, array size (N) of ~3000 (35x86) 'tube' sections, and a 5 cm diameter focusing lens (A_{lens}). The feasibility of these parameters is discussed in a following section.

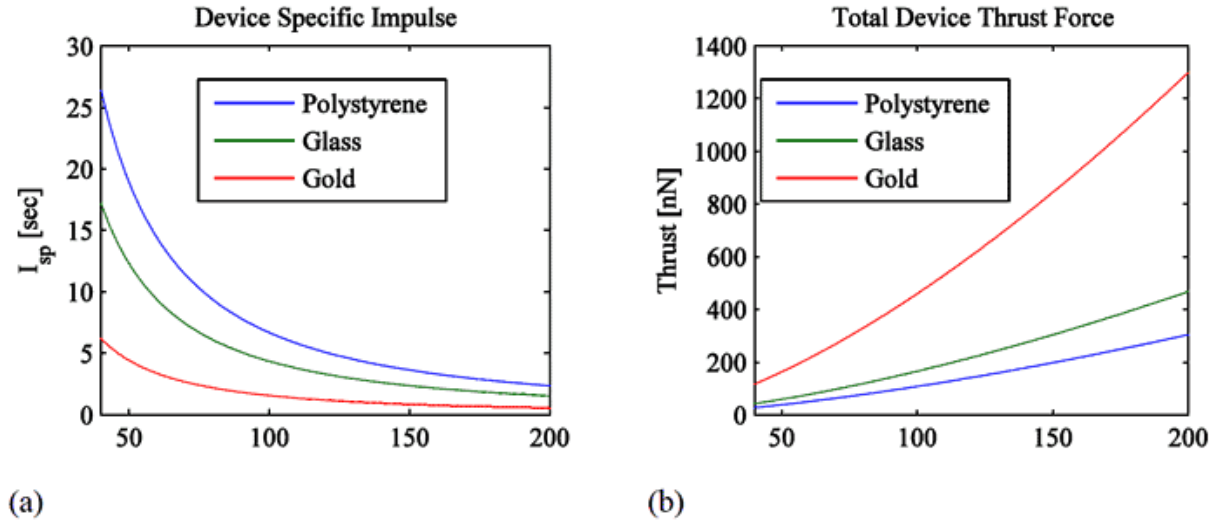

Figure 12: Performance analysis of the conceptual plasmonic thruster, calculated using a 5 mm acceleration length in an 86 by 36 layer thruster array. (a) Comparison of the specific impulse. (b) Thrust comparison of each propellant.

Increasing the acceleration length (L) does not increase the thrust or specific impulse. A longer acceleration length does increase the thrust and the specific impulse for a constant incident light power, as shown in Eqn. 11. But as acceleration length increases, the total area of the nanostructure array (i.e., $A_{thruster}$) also increases. As Eqn. 10 shows, this will reduce the power incident on the thruster, resulting in decreased plasmonic force. The increase provided by longer acceleration lengthis cancelled by the decrease in light power incident on the thruster.

An identical trend is found for the array size (N). Increasing the array size (N) does not increase the thrust. Array size also has no impact on specific impulse. A larger array size would increase thrust for a constant incident light power, as shown in Eqn. 12. But as array size increases, the total area of the nanostructure array (i.e., $A_{thruster}$) also increases. As Eqn. 10 shows, this reduces the power incident on the thruster, resulting in decreased plasmonic force. The increase provided by a larger array is cancelled by the decrease in light power incident on the thruster.

Expulsion rate (f) does directly impact the thrust, but has no impact on specific impulse, as shown in Eqn. 12 and 13. Thrust increase linearly with expulsion rate. Specific impulse is a measure of the exit velocity, and the rate at which particles are being expelled does not effect their final velocity. Expulsion rate is estimated to be 1x10^6 per second for the analysis here, based on previous studies of nanoparticle extraction using gas jets [11]. We have also investigated other methods for loading nanoparticles into the thruster and controlling nanoparticle expulsion rate. These are discussed in the "Additional Considerations" section below.

Thrust and specific impulse are greatly affected by the light power incident on the nanostructures. That is, by the size of the collection lens used to focus solar light onto the thruster, A_{lens}. There is a linear relationship between lens diameter and thrust and specific impulse, as shown in Figure 13. This is a direct result of Eqn. 10, where the lens area directly increases the incident power on the thruster, which increases the plasmonic force, total nanoparticle acceleration, exit velocity, specific impulse, and thrust. The relationship is linear because of the proportionalities in the above equations, which is summarized here. The solar power incident on the thruster is proportional to the lens area, which is proportional to the square of the lens diameter (Eqn. 10). The power incident on the thruster is also proprtional to the plasmonic force generated by the the nanostructures, which is proportional to the square of the exit velocity (Eqn. 11) and square of the specific impulse and thrust (Eqn. 12 and 13). Therefore lens diameter should be linearly related to the thrust and specific impulse, which is what the model results show (Figure 13).

$$P_{thruster} \propto A_{lens} \propto d_{lens}^2 \propto F_{plasmonic} \propto v_{exit}^2 \propto I_{sp}^2 \propto T^2$$

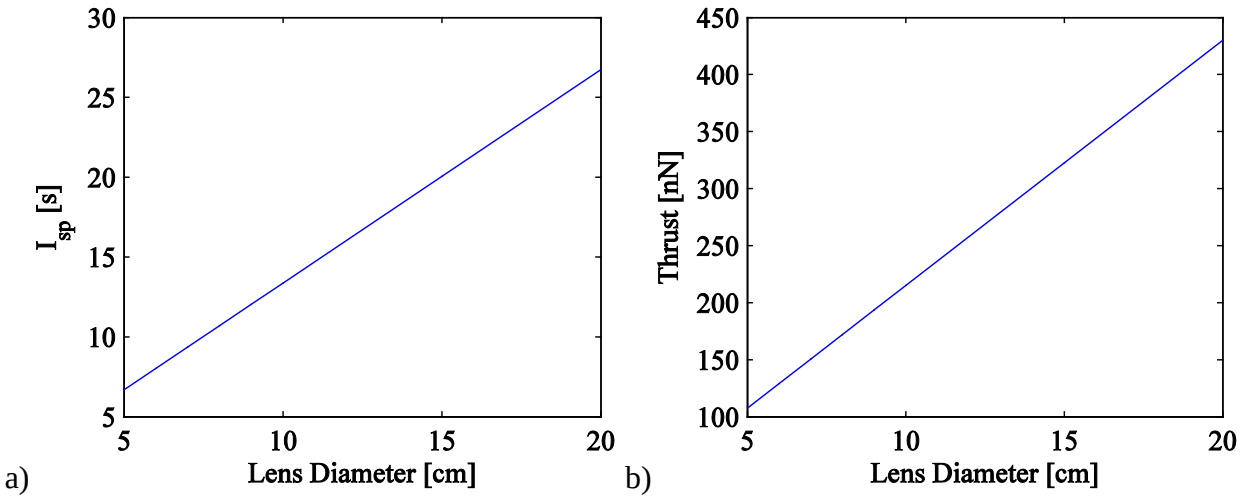

Figure 13: a) Specific impulse and b) Thrust vs Lens Diameter for 100 nm polystyrene nanoparticles.

4. Main Conclusions

A plasmonic force propulsion thruster should have a specific design geometry and configuration, and we have created a conceptual design. A single plasmonic force propulsion thruster should consist of many individual asymmetric nanostructures arranged in a multi-stage, layered, array. Nanostructures should be arranged end-to-end in series to form a multi-stage because a single nanostructure produces very small force and multiple stages are necessary to achieve useable thrust and exit velocity. Multi-stage nanostructures should be layered (i.e., stacked) on top of each other. Each layer should be designed to resonate at a different wavelength within the broadband solar spectrum. This will maximize use of the broadband solar spectrum as shorter wavelength light is absorbed/resonates with top layers, while longer wavelength light passes through to resonate with lower layers. Finally, the multi-stage layers of nanostructures should be repeated in an array to provide increased thrust.

One possible design could use 100 nm diameter polystyrene nanoparticles, a 5 mm acceleration length (L), particle expulsion rate (f) of $1x10^6$, array size (N) of ~3000 (35x86) 'tube' sections, and a 5 cm diameter focusing lens (A_{lens}). This thruster would generate a total thrust of 250 nN at a specific impulse of 10 sec. The array of ~3000 multi-stage nanostructures corresponds to width of ~40 microns. By comparison, the average width of a human hair is ~70 microns. Further, this system offers a fair amount of flexibility for application on a small spacecraft, as performance metrics can be varied by expulsion rate, propellant choice, and lens collection area. Additionally, any increases to lens size, and thus the incident solar power will improve performance of the device.

C. Specific Objective 3: Position and Pointing Precision Capability

We evaluated position control resolution and pointing precision of plasmonic force propulsion for nano/pico-satellites. Attitude control simulations using a bang-bang control algorithm are used to compare different types of thrusters and torquers for small spacecraft.

The reason for selecting fine pointing and positioning mission context is that The National Research Council [12], in reviewing NASA's In-Space Propulsion System Roadmap [7], selected micro-propulsion as a high-priority technology and stressed the need for "non-chemical propulsion that fulfills the needs for high mobility micro-satellites (<100 kg) and extremely fine pointing and positioning for certain astrophysics missions." Propulsion that enables precision positioning can enable or improve a broad class of scientific missions, such as a single Earth observing spacecraft, deployable x-ray telescopes, exoplanet observatories, and constellations of spacecraft for Earth and deep space observations. One of the most prominent examples is the Laser Interferometer Space Antenna (LISA) mission,[*] which uses a constellation of three ~400 kg mini-spacecraft to support picometer displacement measurements to detect gravity waves from super massive black hole mergers [13]. Additionally, future NASA missions are envisioned that will require very fine pointing precision, with resolution as fine as 0.1 mas (milliarcsecond) (

1. Bang-Bang Control Algorithm and CubeSat ACS Model

Three separate programs were written in MATLAB to simulate three different control scenarios; attitude control using RCS thrusters, proximity control using RCS thrusters, and attitude control using reaction wheels. Each of these scenarios involves the cubeSat employing a *bang bang* or "On/Off" control algorithm to move to or maintain a desired position or attitude in the presence of Solar Radiation Pressure (SRP).

Qualitative Description of Implementation of Bang-Bang Control Algorithms

The codes for the attitude and position control simulations presented in this study was written in MATLAB and the algorithms are as follows. The user inputs mass and size of a cubeSat, as well as the thruster moment arm, thrust, number of thrusters, specific impulse, and the switching time of the thruster to be tested. The worst case scenario solar radiation torque or force is calculated using the cubeSat size as described in a following section. The user then defines an initial attitude/position, initial velocity, a desired attitude/position, and switching interval.

The body of the code is a "for" loop where each iteration calculates the satellite current position or attitude, and is illustrated by the flow chart in Figure 14. In each iteration the thruster is either

[*] http://lisa.nasa.gov/

on or off for the switching time of the thruster. The simulation keeps track of the spacecraft attitude/position and velocity, and decides whether or not it is necessary to fire the thruster and in which direction the thruster should be fired to keep the satellite at the desired attitude/position. It is assumed that the satellite sensors measure the attitude/position and the angular velocity/linear velocity with zero error. If the current attitude/position is outside of the switching interval then the spacecraft fires its thrusters in the appropriate direction to arrive at the set attitude/position. The spacecraft constantly calculates the distance it will take to stop if it decelerated constantly from its current velocity to zero. When that distance equals the distance away from the set attitude/position the spacecraft will decelerate to zero velocity. If the attitude/position is inside the switching interval the spacecraft measures its velocity. If the velocity is greater than the smallest change in velocity the thrusters are capable of producing and the velocity and pointing error are both positive or both negative (meaning the attitude vector is moving away from the desired attitude) then the thrusters will fire in order to nudge the spacecraft back toward the desired position/attitude.

Throughout the simulation the current attitude/position, velocity, torque/force, and propellant consumption are recorded and plotted. If the thruster is not capable of keeping the attitude/position of the satellite within 10% of the switching interval a warning will be displayed stating that the current thruster is not capable of maintaining the switching interval desired.

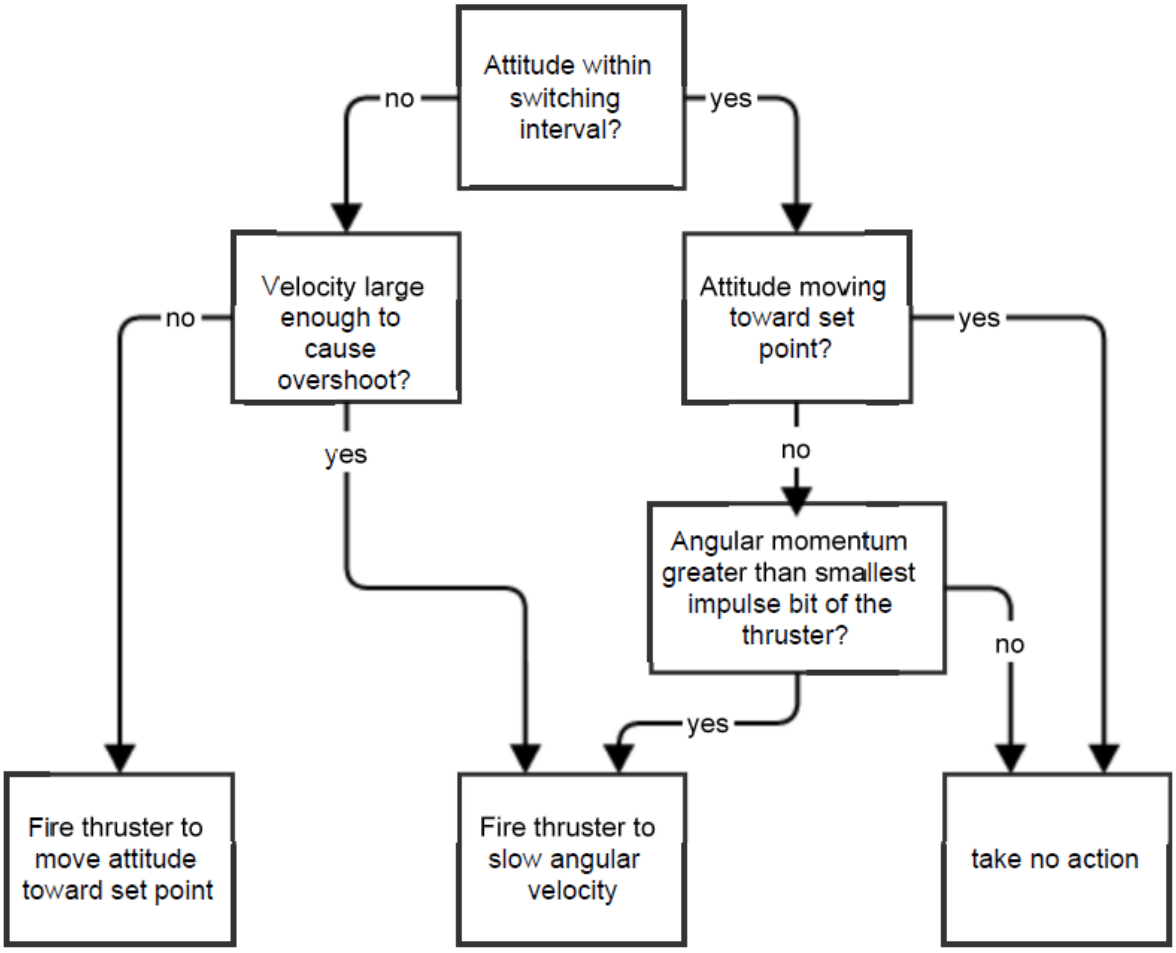

Figure 14: Flow chart outlining the PD bang-bang control algorithm used for attitude control. The same flow chart can used for proximity control by simply replacing the words attitude, angular momentum, and angular velocity with position, momentum, and velocity respectively.

Modeling Solar Radiation Pressure

In space there are a number of forces which can perturb the attitude and orbit of a spacecraft. If the spacecraft is sufficiently long then the end closer to the earth will experience a greater gravitational force then the end farther away causing a tidal torque. Similarly the earth's magnetic field can exert tiny torques on a spacecraft changing its attitude. A large mountain range or other geographic feature may alter the earths local gravitational field changing the spacecraft orbit. Also, in low earth orbit there are still some remnants of the earth's atmosphere which exert a slight aerodynamic drag. However, above 400 km the largest disturbing on a spacecraft's attitude is solar radiation pressure (SRP) [14]. SRP is also one of the largest disturbing forces on satellites formation flying while in the same orbit.

SRP is the force from sunlight striking the surface of a spacecraft. The force acting on a surface is given by integrating

$$d\boldsymbol{f}_{SRP} = -\frac{F_e}{c}\left[(1 - C_s)\hat{\boldsymbol{S}} + 2\left(C_s\cos(\theta) + \frac{1}{3}C_d\right)\hat{\boldsymbol{N}}\right]\cos(\theta)dA$$

over the illuminated surface. Where F_e is the intensity of the light (1358 W/m^2 at 1 AU), c is the speed of light, C_s is the fraction of light which is specularly reflected, C_d is the fraction of light which is diffusely reflected, $\hat{\boldsymbol{S}}$ is the direction of light propagation $\hat{\boldsymbol{N}}$ is the direction normal to the surface, θ is the angle between $\hat{\boldsymbol{S}}$ and $\hat{\boldsymbol{N}}$, and dA is the area to be integrated over.

For a 1U cubeSat the worst case scenario solar radiation *force* is when one face of the cubeSat is directly facing the sun such that $\theta = 0$. Then the force is given by

$$\boldsymbol{F}_{SRP} = -2\frac{F_e}{c}A\hat{\boldsymbol{N}}$$

Where A is the area of the face of the cubeSat facing the sun. For a 1U cubeSat at 1 AU the worst case scenario solar radiation pressure is approximately 90.6 nN.

The worst case scenario solar radiation *torque* is when one face of the cubeSat is directly facing the sun and one half is specularly reflecting 100% of the incident light and the other half is completely shaded. In this case the torque on the space craft is given by

$$\tau = \frac{1}{4}\frac{F_e}{c}AL$$

Where L is the length of one side of the cubeSat. For a 1U cubeSat at 1AU the worst case scenario solar radiation torque is approximately 1.13 nN·m.

Proximity Control Using Reaction Control Thrusters

This section describes in detail the mathematical model used to model position control using RCS thrusters. Due to length constraints the MATLAB code has been omitted. The assumptions of this model are as follows:

1. There are no outside forces affecting the motion of the spacecraft other than its thrusters and solar radiation pressure.
2. This is a single axis simulation so all forces (thrust and SRP) act only along that axis.
3. The spacecraft always knows its current position and velocity with perfect accuracy.
4. The point/object/other satellite which the spacecraft is trying to maintain proximity to is inertially fixed.
5. SRP is constant and is calculated for the worst case scenario where the Sun is directly behind the spacecraft and the spacecraft surfaces reflect light perfectly back toward the Sun.
6. The attitude of the spacecraft remains constant such that one face of the cubeSat is directly facing the Sun.
7. The spacecraft is a cube with constant density.
8. For every time step of the simulation the thrusters can either be fired or not fired. There is no recharge time for the thrusters and each burst delivers the exact same impulse bit for the specified switching time.
9. Because fuel consumed during simulations is very small (usually less than 1 mg) the spacecraft is assumed to have constant mass.

Spacecraft inputs are its mass, M in kg, and the length of a side of the cubeSat, L in m. Thruster inputs are thrust, F in N, switching time, t in s, specific impulse, Isp in seconds, number of thrusters, n, and the mass of on board propellant, Mp in kg.

The spacecraft is assumed to be under constant acceleration from SRP given by the previous section. For a 1U cubeSat with one face directly facing the Sun FSRP = 90.6 nN. The acceleration due to solar radiation and due to the thrusters being fired is easily calculated using Newtons second law.

Next after initializing the position, velocity and desired position the simulation begins. Each iteration represents a time step lasting for the switching time t. During each iteration the bang-bang algorithm decides whether to fire the thrusters in the +x direction or the -x or to take no action. Also, each iteration the distance required for the spacecraft to stop at its current velocity is calculated using the basic kinematic equations found in any elementary physics text [16],[17].

$$x_{stop} = \frac{1}{2}\frac{V^2}{a_{thrust}} \tag{14}$$

In the case where the spacecraft is outside of the switching interval but moving toward the desired position this number is used to decide whether the thrusters should continue firing toward the desired position or fire the opposite direction bringing the spacecraft to a stop. After deciding whether or not to fire the thrusters and in what direction the current position and velocity of the spacecraft is updated.

$$x_{new} = x_{old} + \frac{1}{2}a_{thrust}t^2 + \frac{1}{2}a_{SRP}t^2 + V_{old}t \tag{15}$$

$$V_{new} = V_{\boldsymbol{old}} + a_{thrust}t + a_{SRP}t \tag{16}$$

Where a_{thrust} = +/-nF/M or 0 depending on whether or not the thrusters are being fired and in which direction. Finally the total time the thrusters have been operating, T is recorded and the mass of propellant which has been expended, Me is calculated using [18]

$$M_e = \frac{nFT}{gI_{sp}} \tag{17}$$

Plots of the spacecraft's position and velocity, as well as the force produced by the thrusters, the error in the position and velocity, and the propellant consumed are produced. A sample output of the simulation is provided in Figure 15. The sample output shown in Figure 15 was simulating a 2 kg 1U cubeSat with two PFP thrusters producing 250 nN of thrust with a switching time of 1 ms. The cubeSat moved 10^{-10} m then held position within a switching interval of $2x10^{-12}$ m all while under a 90 nN disturbance force from SRP.

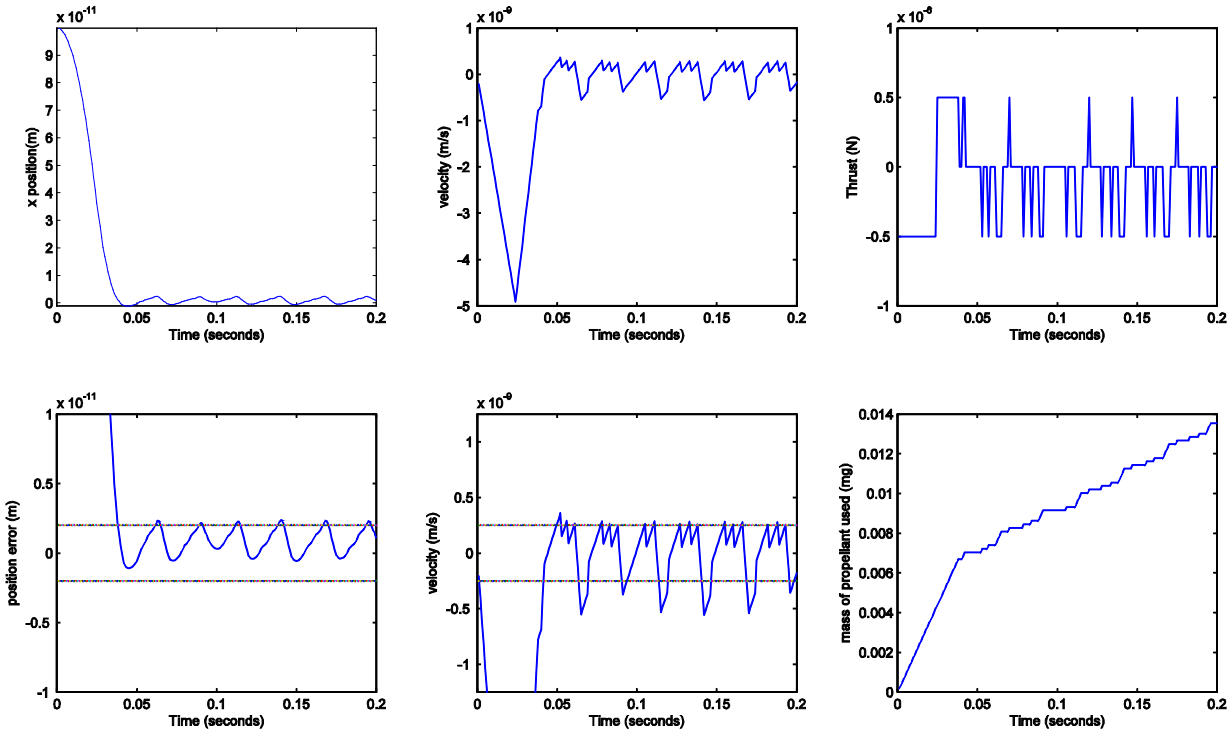

Figure 15: Sample output of proximity control simulation.

Limitations of RCS model.

At this point the assumption of knowing position and velocity to perfect accuracy begins to break down. The most accurate laser interferometers can only measure lengths to within a fraction of a wavelength of light.[19] Interferometers exist which can measure sub-angstrom lengths but they aren't the sort of instruments which would easily fit on a cubeSat.[20],[21] However, the purpose of the simulation is not to determine the actual positioning accuracies, but the theoretical limits of positioning accuracy.

While it may not be possible for cubeSats to fly with such precision NASA is currently developing the technology to allow the three spacecraft of the Laser Interferometer Space Antenna or LISA mission to be able to detect their position relative to each other with picometer precision. The mission of LISA is to detect and pinpoint sources of gravitational waves in space. In order to do this the LISA spacecraft must be able to detect changes in the distance between each spacecraft on the order of tens of picometers over 5,000,000 km! The requirements for the thrusters currently being developed for these spacecraft is that they have a thrust of 5-30 μN. [22-24] An array of tens of PFP thrusters would be able to produce thrusts on that level making PFP thrusters a possible option for the LISA mission. While a single PFP thruster producing thrusts on the level of 50-500 nN could allow for even higher positioning accuracies on future NASA missions.

Attitude Control using Reaction Control Thrusters

This section describes in detail the mathematical model used to model attitude control using RCS thrusters. The MATLAB code implementing this model may be viewed in Appendix B. The assumptions of this model are as follows:

1. There are no outside forces affecting the rotation of the spacecraft other than its thrusters and torque from solar radiation pressure.
2. This is a single axis simulation so all torques (thrust and SRP) act only along that axis of rotation.
3. The spacecraft always knows its current angular position and angular velocity with perfect accuracy.
4. Solar radiation torque is constant and is calculated for the worst case scenario where the Sun is directly behind the spacecraft, and half of the surface facing the Sun reflects its light perfectly and the other half is shaded. All attitude changes are small such that the torque from SRP remains constant
5. The spacecraft is a cube with constant density.
6. For every time step of the simulation the thrusters can either be fired or not fired.
7. There is no recharge time for the thrusters and each burst delivers the exact same impulse bit for the specified switching time.
8. Because fuel consumed during simulations is very small (usually less than 1 mg) the spacecraft is assumed to have constant mass.

Spacecraft inputs are its mass, M in kilograms, and the length of a side of the cubeSat, L in meters. Thruster inputs are thrust, F in Newtons, switching time, t in seconds, specific impulse, I_{sp} in seconds, number of thrusters, n, and the moment arm of the thrusters $r = L/2$ in meters. For attitude control using RCS thrusters at least two thrusters must fire simultaneously on both sides of the spacecraft to prevent any translation.

Next the physical characteristics of the spacecraft, or the *plant* of the control system are calculated. Since the cubeSat is assumed to be a cube of constant density its moment of inertia is give by [16],[17]

$$J_{sat} = \frac{1}{6}ML^2. \tag{18}$$

The torque produced by the thrusters when they are firing is given by [16],[17]

$$\tau_{thrust} = nrF \tag{19}$$

Thus the angular acceleration of the spacecraft when the thrusters are firing is given by

$$\alpha_{thrust} = \frac{\tau_{thrust}}{J_{sat}} \tag{20}$$

Next the *worst case scenario* disturbance torque from solar radiation pressure is calculated from Eq (21)

$$\tau_{solar} = \frac{1}{4}PAL. \tag{21}$$

Eq (21) evaluated for a 1U cubeSat with $L = 10$ cm, and $A = 100$ cm^2, gives $\tau = 1.13 \times 10^{-9}$ N·m. Thus the angular acceleration due to SRP is

$$\alpha_{solar} = \frac{\tau_{solar}}{J_{sat}} \tag{22}$$

With all of the preliminary calculations done the attitude control simulation begins as described above. Each iteration again represents one time step equal to the switching time of the thruster system. The angular distance required to stop the spacecraft rotation at its current angular velocity is calculated every iteration using

$$\theta_{stop} = \frac{1}{2}\frac{\omega^2}{a_{thrust}} \tag{23}$$

where ω is the cubeSats current angular velocity. In the case where the spacecrafts attitude is outside of the switching interval but moving toward the desired attitude this number is used to decide whether the thrusters should continue firing toward the desired position or fire the opposite direction bringing the spacecrafts rotation to a stop. After deciding whether or not to fire the thrusters and in what direction the current attitude and angular velocity of the spacecraft are updated.

$$\theta_{new} = \theta_{old} + \frac{1}{2}\alpha_{thrust}t^2 + \frac{1}{2}\alpha_{solar}t^2 + \omega_{old}t \tag{24}$$

$$\omega_{new} = \omega_{old} + \alpha_{thrust}t + \alpha_{solar}t \tag{25}$$

Where θ is the spacecrafts attitude, ω is its angular velocity, and t is the switching time of the thruster. $\alpha_{thrust} = \pm\frac{nF}{M}$ or 0 depending on whether or not the thrusters are being fired and in which direction. Finally the total time the thrusters have been operating, T is recorded and the mass of propellant which has been expended, M_e is calculated using [18]

$$M_e = \frac{nFT}{gI_{sp}}. \tag{26}$$

A sample output of the attitude control simulation is shown in Figure 16, showing how the spacecrafts attitude, and angular velocity vary with time as well as when the thrusters fire and the propellant usage. The simulation shown in Figure 3 was for two PFP thrusters mounted on either side of a 2 kg 1U cubeSat scaled such that their thrust was only 50 nN. The thrusters also had a specific impulse of 2.9 s, and a switching time of 1 ms. The cubeSat rotated a distance of 5×10^{-8} degrees which is 1.8×10^{-4} arc-seconds then came to a stop and maintained a switching interval of 1×10^{-9} degrees or 3.6×10^{-6} arc-seconds in the presence of SRP. The solar radiation torque was pushing the cubeSat in the $+\hat{\theta}$ direction which is what caused it to overshoot as it approached the set attitude of zero degrees.

Limitation of ACS model

While the thruster may be theoretically capable of maintaining a switching interval of 1×10^{-9} due to the relative strength of the thruster torque, and solar radiation pressure torque the assumption of knowing angular position to perfect accuracy breaks down. Assuming the cubeSat was using some sort of optical telescope mounted on it for attitude sensing it would not even be able to sense the 5×10^{-8} degree attitude change shown in Figure 16 because of diffraction. Because of the wave nature of light, diffraction limits the angular resolution of any optical instrument. The smallest angle which can be resolved by an optical instrument is given by

$$\phi_d = \sin^{-1}(1.22\frac{\lambda}{a}) \tag{27}$$

where ϕ_d is the diffraction limited angle λ is the wavelength of light observed and a is the diameter of the aperture of the optical instrument. [19],[25] Thus even if the cubeSat was fitted with a diffraction limited $a = 10$ cm diameter ultraviolet telescope sensing light with wavelengths of $\lambda = 1$ nm the best angular resolution achievable by that telescope would be $\phi_d = 7 \times 10^{-7}$ degrees! Even so, if PFP thrusters were to be employed on a cubeSat or larger satellite such as a space telescope they would be able to provide a pointing accuracy which was limited by the spacecraft attitude sensing instruments not by the attitude control thrusters.

One proposed NASA mission which requires an extremely high pointing precision of 0.1 milliarcseconds is The Stellar Imager. This space based ultraviolet telescope will have over 200× the resolution of the Hubble Space Telescope and will be able to take images showing details on the surfaces of other stars. The Stellar Imager will consist of 20-30 small "mirror sats" flying in formation to produce a giant mirror. To to this each "mirror sat" will need to be placed with nanometer precision and control its attitude with milliarcsecond precision. The mission concept is still under development, but it is clear that The Stellar Imager will need extremely fine pointing capabilities which could be provided by enabling technologies such as PFP thrusters.[26-28].

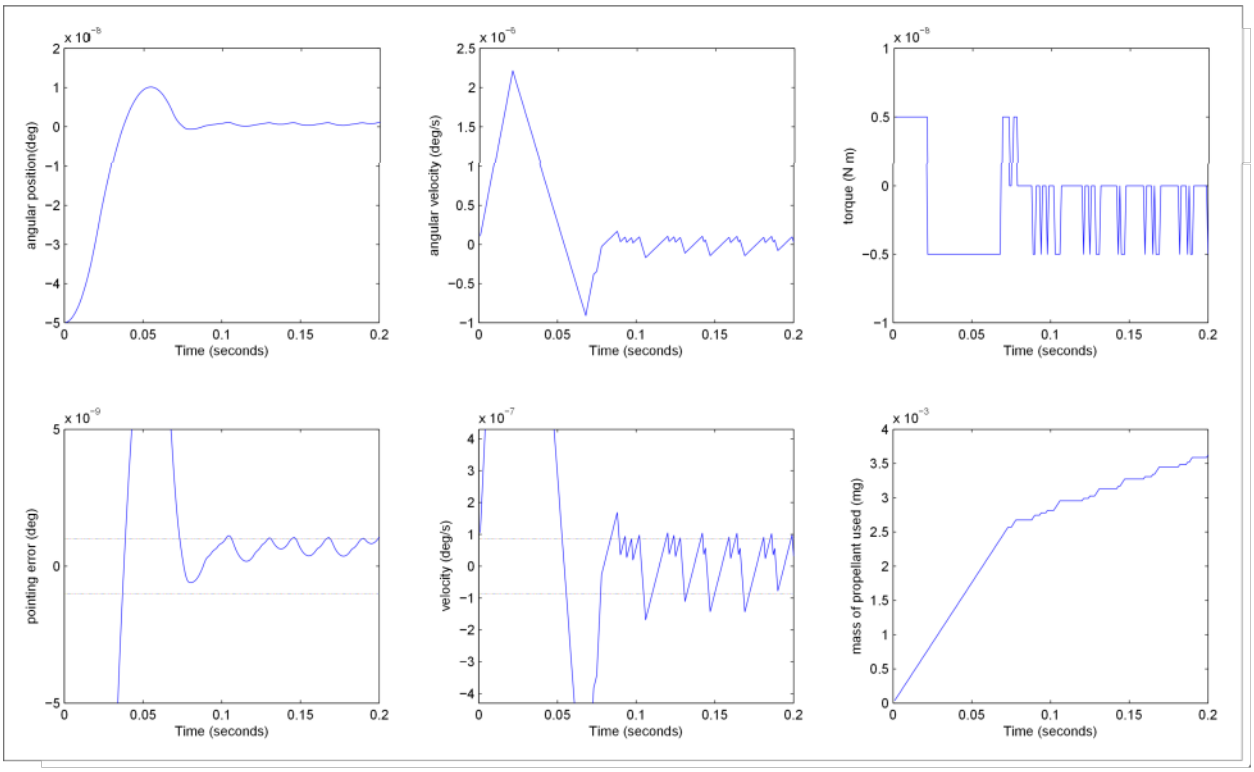

Figure 16: Sample output of attitude control simulation.

Attitude Control Using Reaction Wheels

Reaction wheels are an attitude control mechanism which use the law of conservation of angular momentum to control the rotation of a satellite. A reaction wheel is simply a fly wheel which has its angular velocity constantly controlled by an electric motor. Since the angular momentum of the satellite–reaction wheel system is conserved, when the motor produces a torque on the reaction wheel a counter torque equal in magnitude and in the opposite direction is applied to the satellite. The primary characteristics of reaction wheels which determine its pointing accuracy are its moment of inertia, and the precision with which it can maintain a certain rotation rate.[29-32]

Since reaction wheels have variable torque generally models of control systems use a Proportional Integral Derivative or PID feedback control model. However, such models, while excellent for controlling attitude maneuvers, will yield the non physical result of zero steady

state pointing error. [33],[55] Because of this a model almost identical to the *bang bang* control model used in Section 2.5 will be used. In this model the reaction wheel will be operated in *minimum torque mode*. As the name implies in this mode there will be one magnitude of torque on the reaction wheel which corresponds to the minimum amount the reaction wheels angular velocity can be changed. As a result this model will not be useful for determining the minimum time it takes for the spacecraft to perform a certain maneuver. Rather this model determines the minimum pointing error possible for a particular reaction wheel.
The assumptions of this model are as follows:

1. There are no outside forces affecting the rotation of the spacecraft other than the torque from the reaction wheel and torque from solar radiation pressure.
2. This is a single axis simulation so all torques (from the reaction wheel and SRP) act only along that axis of rotation, it is also assumed that only one reaction wheel is on the spacecraft.
3. The spacecraft always knows its current angular position and angular velocity with perfect accuracy.
4. Solar radiation torque is constant and is calculated for the *worst case scenario* where the Sun is directly behind the spacecraft, and half of the surface facing the Sun reflects its light perfectly and the other half is shaded.
5. All attitude changes are small such that the torque from SRP remains constant.
6. The spacecraft is a cube with constant density.
7. For every time step of the simulation the reaction wheel can either be torqued upon or not. Each torque put on the reaction wheel has the exact same magnitude but may alternate direction.
8. The reaction wheel is operated in "minimum torque mode" where only enough torque is placed on it to change its RPMs by the minimum amount possible.

The model begins in the same way as attitude control model where the user specifies the mass and size of the cubeSat. The user then specifies the properties of the reaction wheel including: moment of inertia, J_{rw}, the minimum amount which the reaction wheels angular momentum can be changed, $\Delta\omega_{rw}$ in revolutions per minute (RPM) (later converted to radians per second), and the *reaction time*, t which is the time it takes the motor of the reaction wheel to change its speed by $\Delta\omega_{rw}$ in seconds. If the moment of inertia is not specified by the manufacturer then it may be approximated by the formula

$$J_{rw} = mR^2 \tag{28}$$

where m is the mass of the wheel in kilograms, and R is the radius of the wheel. This formula assumes that all of the mass of the reaction wheel is concentrated along the rim of the wheel.[16],[17] Next the minimum amount which the cubeSat angular velocity can be changed is calculated using

$$\Delta\omega_{sat} = \frac{J_{rw}\Delta\omega_{rw}}{J_{sat}} \tag{29}$$

where J_{sat} is the moment of inertia of the cubeSat given previously by Eq (18).[16],[17],[32] Thus from basic kinematics the angular acceleration on the satellite is given by

$$\alpha_{sat} = \frac{\Delta\omega_{sat}}{t} \tag{30}$$

The torque on the sat from the reaction wheel is

$$\tau_{sat} = J_{sat}\alpha_{sat} \tag{31}$$

The torque and acceleration from SRP is exactly the same as was calculated in Eqs (21) and (22).

The simulation runs the same as was described above with each time step lasting for the *reaction time* t. When the algorithm decides whether to apply a positive or negative torque on the spacecraft the current position and velocity are updated using Eqs (24) and (25) while the speed of the reaction wheel is updated using

$$\omega_{rwnew} = \omega_{rwold} \pm \Delta\omega_{rw} \tag{32}$$

A sample output of the simulation is provided in Figure 4. This simulation corresponded to a 1U 2 kg cubeSat with a 50 g, 20 mm radius reaction wheel. The reaction time of the wheel was 0.1 s and the satellite successfully maintained a switching interval of 0.02 degrees.

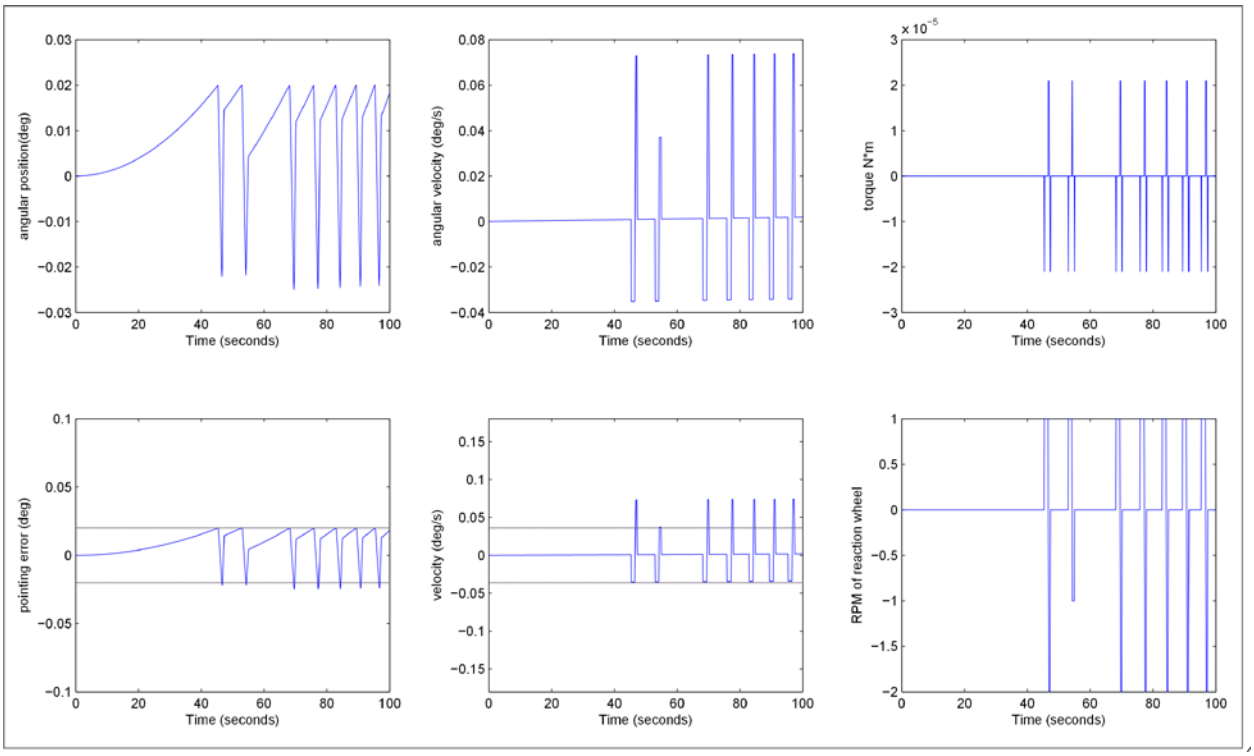

Figure 17: Sample output of attitude control simulation using reaction wheels.

2. Position and Pointing Comparison of Different Thrusters and Torquers

Several new and developing micro propulsion systems for small satellites were studied and modeled using the algorithms presented in the section above. This section documents the characteristics of each thruster system and compares its performance to that of plasmonic force thrusters. The results of the simulations and a comparison of the characteristics of each thruster is summarized in the last part of this section.

Plasmonic Force Propulsion (PFP) Thrusters

Plasmonic Force Propulsion (PFP) thrusters are a novel new small sat RCS which function by using the light from the Sun to accelerate nanoparticles at high speed. The plasmonic force being used by the thruster to accelerate nanoparticles is similar to the optical force produced by the

"optical tweezers" which biologists use to move viruses around.[33],[34]. Optical tweezers work by using the electric field gradient produced by a focused laser to move dielectric nanoparticles to the waist of the beam where the electric field is the strongest. PFP thrusters also use electric field gradients produced by light to accelerate nanoparticles, but are different from optical tweezers in that the electric field gradient is not produced by the concentrated light itself but rather by the interaction of the light with a nanostructure. It has been shown that plasmonic forces created by the interaction of light with metallic nanostructures can trap nanoparticles, [35],[36], but accelerating nanoparticles to create thrust has not yet been widely researched. Also, it should be noted, since there has previously been much confusion about this, that the interaction between light and the nanostructures produces a *potential ramp* not a *potential well*. Simulations of the potential profile and force on nanoparticles for novel asymmetric geometry nanostructures were shown in Figure 6 and Figure 7. A conceptual PFP device is shown in Figure 8 and performance parameters were estimated and shown in Figure 12 and Figure 20.

The size, configuration, and propellant type of PFP thrusters will be easily customizable to fit the needs of various missions. In this study a single thruster configuration consisting of an array of 3010 (35x86) devices, 5 mm long acceleration length, with each tube expelling 1×10^6 100 nm diameter polystyrene nanoparticles per second was used to obtain baseline thrust and specific impulse estimates. This baseline thruster is 35 nanotubes thick and 86 wide, on the top and bottom of each nanotube is a plasmonic nanostructure each designed to resonate with a different wavelength of light ranging from 1100 nm to 400 nm. Such a thruster would have a width of 52 μm and a thickness of 5 μm. By comparison a human hair is 70 μm in diameter. The mass of each thruster would be negligible so the system mass would be determined by the 5 cm diameter lens used to focus the light on the nanostructures and the total mass of the propellant used. It is estimated that such a multistage array plasmonic thruster with all the light from a 5 cm diameter lens focused on it would have a thrust of 107.5 nN and a specific impulse of 6.69 s.

The switching time of PFP thrusters is currently not known and will be determined by how the thruster is actuated. Actuation of the thruster could be controlled by a mechanical shutter or electric glass allowing light to shine on the nanostructures, or an electronically controlled valve on the nanoparticle propellant tank or a combination of these. A mechanical shutter would allow for very fast switching times, high end cameras typically have shutter speeds higher than 1/10,000 of a second. However, the vibrations from a shutter could induce unwanted motion in the spacecraft. Electric glass using "micro-blinds" can change from opaque to transparent and back on the order of a millisecond but is still under development.[37]

Micro-Cathode Arc Thrusters (μCAT)

The Micro-Cathode Arc Thruster (μCAT) is currently under development at The George Washington University and is at TRL-4. The μCAT consists of a titanium cathode and a copper anode separated by an insulator. The copper anode is surrounded by an inductor which releases a high voltage pulse causing a discharge between the electrodes. The titanium cathode acts as the propellant and ablates during the discharge as a portion its surface is converted to plasma. The plasma is then accelerated out of the thruster being directed by the magnetic field of the inductor.[38-40]

The main advantages of the μCAT is that it has high I_{sp} (2000-3500 s), relatively high thrust (100 μN), and low mass (100 g per thruster) [38],[40]. A cubeSat using μCAT thrusters would also require a inductive pulsed power unit adding a mass of approximately 100 g. The titanium cathode acting as propellant has a mass of 40 g and density of 4.5 g/cm ^{3}. Assuming that the entire Titanium cathode is consumed as propellant a 2 kg cubeSat equipped with a μCAT would have 400-700 m/s of ΔV meaning that the cubeSat would be able to easily perform orbital maneuvers besides station keeping. However, the μCAT is currently only estimated to have a lifetime of 10^8 pulses, meaning with an impulse bit of 2 μNs, it will only be able to provide 100 m/s of ΔV to a 2 kg cubeSat. [41] With a switching time of 20 ms the μCAT can provide good pointing and positioning accuracy of 1×10^{-4} deg and 6×10^{-4} m. As a result of the relatively high thrust produced by the μCAT and larger switching time it is not as well suited for missions which require high accuracy pointing and proximity control as PFP thrusters.

Vacuum Arc Thrusters (VAT)

The Vacuum Arc Thruster (VAT) developed by Alameda Applied Sciences Corporation uses a solid metal cathode as the propellant and is considered to be at TRL-5. A vacuum arc is an electric discharge which occurs in a vacuum between a heated cathode and an anode containing the solid metal propellant. A large number of metals are available as propellants including Titanium, Yttrium, Silver, Tantalum, and Tungsten, but the two most common are Titanium and Tungsten having densities of 4.5 g/cm ^{3} and 19.25 g/cm ^{3} respectively. Typically VATs use a 40 g Titanium anode as the propellant. As the electron beam strikes the propellant anode its surface becomes a plasma which is then accelerated away from the thruster at high speed. [42-45]. The VAT has an extremely large throttleable average thrust range of 10 nN to 300 μN a high specific impulse of 1000-3000 s and a fast switching time of 1 ms. The average thrust ranges from 10 nN to 300 μN, but this is done by altering the switching time of the thruster. The range of impulse bits is 10 nNs to 30μNs. Thus the lowest instantaneous thrust assuming a 1 ms switching time is 10 μN.[42]

With the combination of a wide range of throttleable thrusts and a fast switching time of 1 ms the VAT can maintain extremely low switching intervals. If used on a 2 kg cubeSat it could provide precision pointing to 2×10^{-7} degrees and position accuracy up to 4×10^{-11}m. With its high specific impulse it could provide 200-600 m/s of ΔV assuming it consumed the entire Titanium anode as propellant. However, the rated lifetime of the VAT is only 5 million pulses so each VAT is only able to provide 75 m/s of ΔV to a 2 kg cubeSat. In addition to this the VATs 300 g PPU requires 10 W of power to operate.

The main advantages of the VAT are its large throttleable thrust range, low minimum impulse bit, and fast switching time which allow for extremely low switching intervals at the limit of what a cubeSat can sense. However, its relatively short lifetime, high power consumption, and relatively large mass limit its utility on cubeSats.

Pulsed Plasma Thruster (PPT)

PPTs were originally developed in the late 60s and were the first successful electric propulsion system used in space. They are easily scalable and have been used on a number of large satellites as both an ACS and RCS. PPTs commonly use solid PTFE (Teflon) as a propellant. The Teflon

is ablated and converted to plasma through a high voltage electric discharge between two capacitor plates. the plasma is then accelerated away via the Lorentz force. [56]

Clyde Space makes a small electric propulsion system for small satellites called the Pulsed Plasma Thruster (PPT) produces a thrust of 4.5 μN, has a switching time of 0.2 s and a specific impulse of 608 s. The thruster with all supporting systems comes in a $90 \times 90 \times 27$ mm envelope which conveniently fits into the back fourth of a 1U cubeSat.[46] It carries 7 g of Teflon propellant the density of which is 2.2 g/cm^3 which provides 21 m/s of ΔV for a 2 kg cubeSat. The thruster has a lifetime of 1.5 million pulses and is estimated to provide 42 Ns of total impulse. Currently there is no PPT designed to be used as an ACS on cubeSats and is primarily suited for extending the mission life of cubeSats by providing a small amount of ΔV to combat atmospheric drag. The main advantage of PPTs is that they are a flight proven technology, but they are not as small and efficient as newer thruster systems.

Electrospray Thrusters

Electrospray thrusters operate by accelerating electrically charged droplets of ionic liquids at high speeds using high voltage electric fields. Various Electrospray thruster designs vary widely and are constantly being improved. They have previously been used on larger satellites but MIT is currently developing a miniaturized version for use on cubeSats. Electrospray thrusters have a number of advantages such as high thrust (100 μN), high specific impulse (2500-5000 s), and have a short switching time (1 ms). Each thruster is very small, about the size of a penny, and is only a few grams. an exact mass estimate is not available since the thruster is still under development but each one should have a mass under 10 g. Their main disadvantages are that they require a large high voltage power processing unit which draws 10 W of power, occupies a volume of 300 cm^3 and adds 250-300 g to the system mass. MITs miniature Electrospray thrusters are expected to have an extremely long life and should give cubeSats relatively large amounts of ΔV. They will also provide both positioning and attitude control but not to the level of precision of PFP thrusters. [47-50]

Reaction Wheels

Currently there are not many cubeSat reaction wheels available but a new model which came out in the past year is the Blue Canyon Technologies Micro Reaction Wheel. It has a moment of inertia of 28.6×10^{-6} kg·m^2, mass of 150 g, volume of 33 cm^3, and a max torque of 0.6 mN·m. It only requires a maximum of 1 W of power and operates from 5-15 V. The wheel can reach a maximum speed of 6,000 RPM, and is expected to have a lifetime of 3 years. [51] For the purposes of the simulation it was assumed that the reaction wheel had a reaction time of 0.1 s. This gave a pointing accuracy of 0.01 degrees when placed on a cubeSat. Because of the large torques reaction wheels are able to provide they can turn a cubeSat much quicker than micropropulsion thrusters, however, they do not provide as fine of pointing accuracies.

Micropropulsion summary

Table 1 compares the characteristics of all the micropropulsion systems and reaction wheels considered in this report. As many of these thrusters are still in development and/or easily customizable the values presented in this table vary from source to source.

Table 2: Comparison of various cubeSat propulsion systems.

Thruster type	PFP	μCAT	VAT	PPT	Electrospray	Reaction Wheels
Thrust used in Simulations	250 nN	100 μN	10 μN	4.5 μN	100 μN	N/A
Specific Impulse (s)	1-12	2000-3500	1000-3000	608	2500-5000	N/A
Switching Time (ms)	1	20	1	200	1	100
Pointing Accuracy (deg)	2×10^{-9}	1×10^{-4}	2×10^{-7}	N/A	1×10^{-6}	0.01
Position Accuracy (m)	3×10^{-12}	6×10^{-8}	4×10^{-11}	8×10^{-7}	6×10^{-10}	N/A
Min Impulse Bit (nNs)	50 pNs	2 μNs	10 nNs	900 nNs	100 nNs	N/A
Thruster Mass (g)	<0.001	100	90	280	<10	N/A
Supporting Systems Mass (g)	100	100	300	0	250	150
System Volume (cm^3)	50	200	200	220	300	33
Propellant Mass (g)	50-100	40	40	7	20	N/A
Propellant type	Nanoparticles	Metal (Ti)	Metal (Ti or W)	Teflon	Ionic Liquids	N/A
Propellant Density (g/cm^3)	1.04	4.5	4.5	2.2	varies	N/A
Max Power Required (W)	0	5	10	2.7	10	1
ΔV for 2kg cubeSat (m/s)	1-6	100	75	21	250-500	N/A
Lifetime (pulses)	unknown	10^8	5×10^6	1.5×10^6	unknown	three years
Configurable as ACS?	yes	yes	yes	no	yes	yes
Scalable/Customizable?	yes	yes	yes	no	yes	yes
Throttleable?	yes	no	yes	no	yes	yes
High Voltage Required?	no	yes	yes	yes	yes	no

Table 3: Alternate version of Table 2

Thruster type	PFP	μCAT	VAT	PPT	Electrospray	Reaction Wheels
Thrust used in Simulations	250 nN	100 μN	10 μN	4.5 μN	100 μN	N/A
Specific Impulse (s)	1-12	2000-3500	1000-3000	608	2500-5000	N/A
Switching Time (ms)	1	20	1	200	1	100
Pointing Accuracy (deg)	2×10^{-9}	1×10^{-4}	2×10^{-7}	N/A	1×10^{-6}	0.01
Position Accuracy (m)	3×10^{-12}	6×10^{-8}	4×10^{-11}	8×10^{-7}	6×10^{-10}	N/A
Min Impulse Bit (nNs)	50 pNs	2 μNs	10 nNs	900 nNs	100 nNs	N/A
Thruster Mass (g)	<0.001	100	90	280	<10	N/A
Supporting Systems Mass (g)	100	100	300	0	250	150
System Volume (cm^3)	50	200	200	220	300	33
Propellant Mass (g)	50-100	40	40	7	20	N/A
Propellant type	Nanoparticles	Metal (Ti)	Metal (Ti or W)	Teflon	Ionic Liquids	N/A
Propellant Density (g/cm^3)	1.04	4.5	4.5	2.2	varies	N/A
Max Power Required (W)	0	5	10	2.7	10	1
ΔV for 2kg cubeSat (m/s)	1-6	~100	~75	21	250-500	N/A
Lifetime (pulses)	unknown	10^8	5×10^6	1.5×10^6	unknown	three years
Configurable as ACS?	yes	yes	yes	no	yes	yes
Scalable/Customizable?	yes	yes	yes	no	yes	yes
Throttleable?	yes	no	yes	no	yes	yes
High Voltage Required?	no	yes	yes	yes	yes	no

3. Main Conclusions

From our analysis it is clear that plasmonic force propulsion can extend spacecraft pointing and precision control into an entirely new realm. Figure 18 compares PFP with the other types of propulsion investigated. Thruster system mass is 50% smaller and volume is 75% smaller (Figure 18a). While at the same time, PFP can provide attitude control that is over two orders of magnitude more precise (10^{-9} vs. 10^{-7} degrees, or 0.007 vs. 0.7 milliarcseconds) (Figure 18b). Additionally, PFP can provide proximity control that is an order of magnitude more precise (10^{-12} vs. 10^{-11} m), such that the limiting factor becomes the interferometer used to measure the distance between the objects. PFP enables new types of missions that require this level of pointing precision, such as the Stellar Imager (Figure 18b), and proximity control precision, such as LISA (Figure 18b). Finally, it is clear that PFP is beneficial for pointing and proximity control operations that require relatively low delta-V (i.e., not main propulsion for orbit raising where high delta-V is required) (Figure 18c). For low-delta-V maneuvers, like for the Stellar Imager (delta-Vs of mm/s), PFP is ideally suited. In fact, for total mission delta-V of about 3 m/s or less, PFP propulsion saves mass over competing propulsion systems.

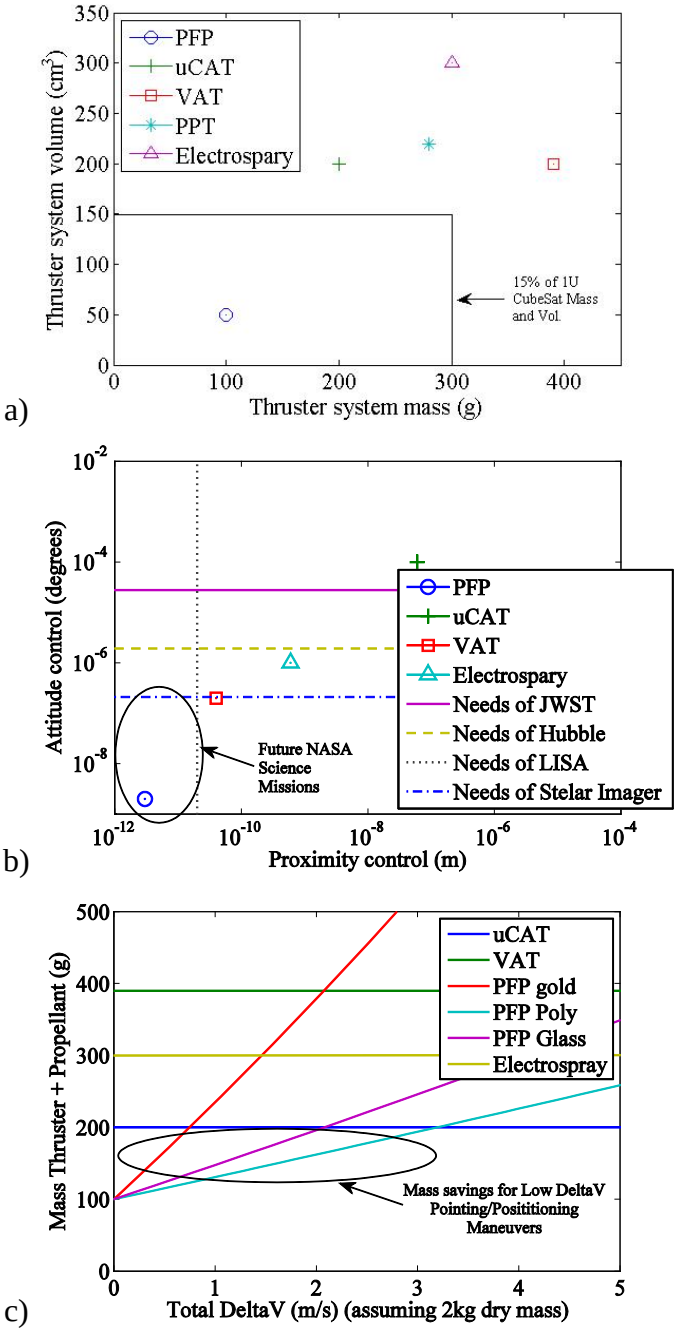

Figure 18: Comparison of plasmonic force propulsion with other state-of-the-art thruster systems. a) Thruster system mass and volume, b) proximity and attitude control capability in comparison with various relevant NASA missions, and c) Thruster and propellant mass as a function of total delta-V for a 2kg dry mass spacecraft

D. Additional Considerations on Plasmonic Propulsion

Throughout the project other questions have come to light, and we have investigated potential solutions for each of them. The following sections describe additional considerations that are important for plasmonic force propulsion.

1. Original Identified Issues and Obstacles

Initially we identified two major issues and obstacles to the concept: (1) the strong light intensity (~mW/μm^2) necessary to generate plasmonic forces (~10-100 pN) and (2) the compatibility of broad band solar light spectrum with the narrow resonance band of plasmonic nanostructure. Our results suggest that issue (2) is not an issue because simulations predict that nanostructures with very narrow resonance band can be designed to interact with light within the broadband solar spectrum. Further, by stacking these nanostructures into layers, smaller wavelengths within the broadband can be absorbed first, while longer wavelengths pass through to be absorbed with lower layers.

Issue (1) relates to the strong light intensity necessary to generate plasmonic forces that can accelerate nanoparticles to appreciable speed. This issue relates directly to the low propulsion performance predicted for PFP, i.e., the low thrust and specific impulse. It is clear that a collection lens is necessary to enhance the 1.4 kW/m^2 available in low-Earth orbit. Our conceptual thruster design incorporates this collection lens and all our performance and control capability modeling accounts for this. The direct result is low specific impulse, which impacts the required propellant to achieve a desired change in spacecraft energy/velocity. But for precision control scenarios where only mm/s of delta-V are required, the low specific impulse has negligible impact on the spacecraft mass (Figure 18c). And our results show that with a realistic lens size of 5-cm-diameter, the control capability provided by PFP far surpasses the existing state-of-the-art (Figure 18 a and b).

2. How Does Light Get to Shaded Thrusters?

One of the most obvious issues with PFP thrusters is how to power thrusters which are in the shadow of the satellite itself. This could be solved by adding a Solar Light Allocation Pipe or SLAP to the PFP thruster system. The SLAP would be a system of fiber optics to pipe light to the needed thrusters something like the design shown in Figure 19. Thrusters are not shown in the figure, but are parallel to the faces of the cubeSat where the fiber optic cables terminate.

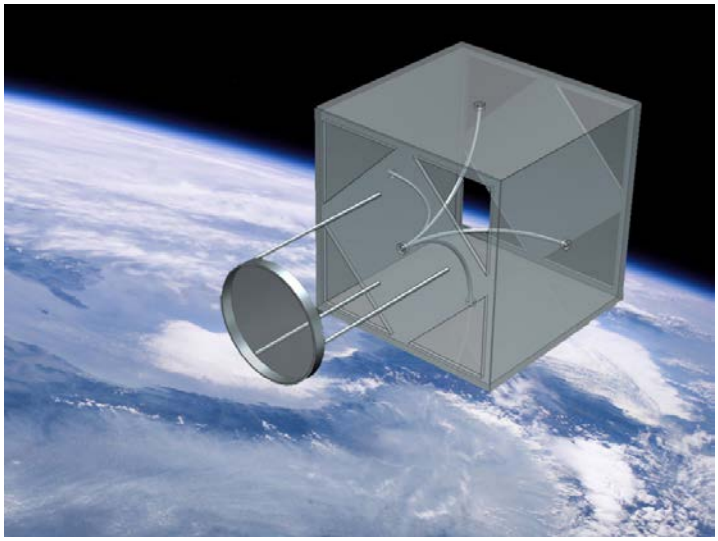

Figure 19: CubeSat over earth using PFP thrusters powered by the SLAP (Solar Light Allocation Pipe).

A SLAP is necessary for precision attitude control and proximity control. In order to perform attitude control maneuvers without changing the satellites orbit, thrusters on both sides of the satellite must be fired simultaneously to null translational motion. This was an integral assumption of the attitude control model. The SLAP is also necessary for proximity control. In order to change position with respect to another satellite a cubeSat must perform two maneuvers to start and stop its motion. Each maneuver will require thrusters on opposite sides of the cubeSat to fire, meaning one of the thrusters will be shaded and unable to fire.

Furthermore, getting the lens to focus the light on the plasmonic thrusters or into the SLAP could prove difficult. In order for Sun light to be focused on a point by a lens the lens must be perpendicular to the incoming rays and the distance between the lens and the point must be equal to the focal length of the lens.[19] As the attitude of the cubeSat changes the lens or the thrusters must move in order to remain in focus. However, adding moving parts will add more mass, volume, complexity, and cost to the system. Furthermore, moving parts will produce a torque on the spacecraft which will decrease pointing accuracy and use up a significant amount of propellant. This would not be an issue on a larger spacecraft employing two separate attitude control systems. If the spacecraft needed to change its attitude, before making the maneuver it could move/rotate the lens such that it would be lined up with the future location of the SLAP. Then the spacecraft could make the maneuver using its primary coarse ACS then use PFP thrusters for fine control.

3. What Happens When in the Shadow of the Earth?

Since PFP thrusters are powered by Sunlight they cannot be operated when in the shadow of the earth or otherwise not illuminated. This is a problem which can only be avoided by placing the spacecraft in an orbit which does not cross into the earths shadow. However, it should be noted that when the spacecraft is in shadow the primary disturbance force, solar radiation pressure, will not be disturbing the spacecraft. Thus, attitude control will not be as critical when operating in the shadow of the earth. Onboard lasers or LED lights could be added to excite the structures producing thrust when in shadow of Earth. But these would add mass/power/volume.

4. Improving Thrust and Specific Impulse

One of the challenges with PFP thrusters is their low specific impulse. The estimated 1-6 m/s of ΔV is ideally suited for proximity and pointing precision control for formation flying with other satellites. But PFP thrusters will not be able to be used to change a spacecrafts orbit or extend the life of cubeSat missions significantly. To use PFP as primary propulsion for orbit raising or orbit change, specific impulse will need to be increased, along with thrust. The best ways to increase specific impulse are to increase the intensity of light striking the nanostructures or to increase the efficiency at which the nanostructures convert light into thrust. Adding a larger lens adds more mass and the small size of cubeSats limits the diameter of any collection lens at 10 cm. Clearly it is more advantageous to have more efficient structures. It is hypothesized that dielectric nanostructures used in hybrid waveguides may be able to provide increased plasmonic forces for the same level of incident solar energy [3].

5. Manufacturing PFP Thrusters

It is currently very difficult to manufacture nanostructures on a macroscopic level. Even making arrays of nanostructures 5 mm long is difficult using current techniques. However, researchers at the Missouri University of Science and Technology are currently working on a new method of manufacturing nanostructures known as *Nanosphere Photolithography* [52-54]. It is hypothesized that this technique could allow nanostructures covering an area as large as 1 m^2 to be produced. If this technique proves to be effective then it would be possible to create PFP thrusters along the entire length of a cubeSat.

6. Achieving High Expulsion Rates

Nanoparticles must be loaded into the thruster from the propellant reservoir. We have identified multiple avenues for accomplishing this, some of which have shown to provide high rates of loading necessary for the concept. High-pressure dispersion has shown that fine powders can be transported by a carrier gas and achieve transport of 10^6 nanoparticles per second [11]. Nanoparticles can be extracted from aqueous solutions at high rate using electric fields, as has been shown in [15]. Finally, it may be possible to use plasmonic forces to manipulate propellant nanoparticles into the thruster. A nanostructure design may be possible that resonantly interacts with solar light to funnel or guide nanoparticles from the propellant reservoir into the accelerating tubes of the thruster.

III. Conclusions

The results for plasmonic space propulsion are very exciting. Plasmonic force propulsion can significantly enhance the state-of-the-art in small spacecraft position and attitude control by 1-2 orders of magnitude. PFP thrusters are a promising new propulsion system for both cubeSats and other small satellites which can be used as both an RCS and ACS. They require no power, and are extremely low mass and volume. Their low thrust and short switching time makes them ideal for missions where exact distances between spacecraft must be maintained or missions which require extremely high pointing capabilities. A cubeSat employing PFP thrusters would be able to maintain at attitude which was only limited by its attitude sensing instruments.

Our results have elucidated the design geometry and configuration for a plasmonic force propulsion thruster, and we have created a conceptual design. A single plasmonic force propulsion thruster should consist of many individual asymmetric nanostructures arranged in a multi-stage, layered, array. Nanostructures should be arranged end-to-end in series to form a multi-stage because a single nanostructure produces very small force and multiple stages are necessary to achieve useable thrust and exit velocity. Multi-stage nanostructures should be layered (i.e., stacked) on top of each other. Each layer should be designed to resonate at a different wavelength within the broadband solar spectrum. This will maximize use of the broadband solar spectrum as shorter wavelength light is absorbed/resonates with top layers, while longer wavelength light passes through to resonate with lower layers. Finally, the multi-stage layers of nanostructures should be repeated in an array to provide increased thrust.

Results for a conceptual design of a plasmonic thruster that has 35 layers, 86 array columns, multi-stage length of 5 mm, a 5-cm-diameter light focusing lens, and uses 100 nm polystyrene nanoparticles expelled at a rate of $1x10^6$ per sec would have a thrust of 250 nN, specific impulse

of 10 sec, and minimum impulse bit of 50 pN-s. The thruster mass and volume are estimated at 100 g and 50 cm^3, respectively.

Plasmonic propulsion is ideally suited for proximity and attitude control maneuvers where the total spacecraft delta-V is relatively small (on the order of 1 m/s, compared with high delta-V orbit raising/maintenance maneuvers ~10-100 m/s). Because of its lower dry mass, plasmonic propulsion has a lower wet system mass for missions requiring delta-V of 3 m/s or less. This is ideal for proximity and attitude control where single maneuvers are mm/s, not main propulsion for orbit raising/maintenance.

The ultra low thrust of PFP thrusters could also be used for attitude or proximity control on larger satellites. NASA's Laser Interferometer Space Antenna mission to detect gravitational waves requires that the satellites know their positions relative to each other and maintain precise orbits to with respect to each other. The LISA spacecraft will not be formation flying and the distance between them will be constantly changing but needs to be constantly known to within 20 pm over 5,000,000 km. As a result, this mission will require extremely precise reaction control thrusters with thrusts on the order of a micro-newton or less.[22-24] PFP thrusters can position a cubeSat accurately to within 3 pm, meaning they could position a larger satellite with greater precision making them a viable option for the LISA mission or future NASA missions which require greater precision.

PFP thrusters are also a viable option for the NASA proposed Stellar Imager or SI mission[†]. This mission concept consists of 20-30 formation flying "mirror sats" each one a meter diameter mirror precisely placed to within 5 nm over several kilometers. Each mirror sat will also have to control its attitude to less than 0.76 milliarcseconds. The entire Interferometer telescope will allow 0.1 milliarcsecond resolution images of stellar surfaces and the universe in general to be taken.[26-28] It is estimated that PFP thrusters can provide pointing accuracy to within 2×10^{-9} degrees or 0.0072 milliarcseconds or 7.2 microarcseconds for a cubeSat. Each mirror sat will be a 1 m diameter mirror segment only a few times larger than a cubeSat so it is reasonable to expect a "mirror sat" employing PFP thrusters to have pointing accuracies comparable to those predicted for a cubeSat.

As a result of our study, the TRL of plasmonic force propulsion has been raised from 1 to 2. We have invented a practical application for the technology: space propulsion. This application is speculative, and our analytical and numerical studies presented here required assumptions without proof or detailed analysis. However, these studies show that plasmonic force propulsion has the potential to provide a 1-2 order of magnitude benefit in the precision pointing and proximity control for small spacecraft.

IV. Future Work

Future efforts should focus on (1) further analyzing the concept within a mission context, (2) experimentally demonstrating nanoparticle acceleration with asymmetric nanostructures excited by the Solar spectrum, and (3) creating a roadmap for future development of supporting technologies. The combination of these future activities would raise the TRL to early 3.

[†] http://hires.gsfc.nasa.gov/si/

The concept should be further analyzed within a mission context. An example specific nano/picosat mission should be determined and analyzed through detailed orbital dynamics calculations. This should include the effects of passing through Earth shadow, if necessary. A possible example mission might be the Stellar Imager, where nanometer level proximity control and 0.1 milliarcsecond pointing control are required between multiple nanosatellites.

Nanoparticle acceleration should be demonstrated experimentally using asymmetric nanostructures excited by the Solar spectrum. Individual asymmetric nanostructures relevant to plasmonic propulsion should be fabricated and characterized. Specifically the transmission spectrum of the nanostructure within the Solar spectrum should be characterized and compared with our numerical predictions reported here. Additionally, nanoparticle manipulation (acceleration) should be characterized and used to determine plasmonic force, which can then be compared with our numerical predictions reported here.

A roadmap should be created for future development of supporting technologies. Supporting technologies necessary for plasmonic propulsion have been investigated here, but a roadmap for future development is necessary. Important supporting technologies include large-scale nanostructure manufacturing, solar light distribution system (fiber optic) development, switching technology development (shutter, microblinds with electric glass), nanoparticle propellant reservoir and feed system development (high-pressure gas, plasmonic manipulation).

V. Notable Outreach Activities

Dr. Rovey participated in the 1st annual Missouri S&T Space Week event by delivering a presentation to undergraduate, graduate, and high school students from the surrounding communities. Dr. Rovey's talk focused on the future of advanced space propulsion, wherein he described the Missouri S&T NIAC team's current activities studying plasmonic force propulsion. http://news.mst.edu/2013/10/spaceweek-at-missouri-st-starts-nov-4/

Students Paul Friz and Matt Glascock attended the 2014 Missouri Space Grant Consortium conference and presented their results on plasmonic force propulsion to graduate, undergraduate, and highschool students from around the State. http://web.mst.edu/~spaceg/index.html

VI. References

[1]Juan, M. L., Righini, M., Quidant, R., "Plasmon nano-optical tweezers," *Nature Photonics*, Vol. 5, No. 6, pp. 349-356, 2011.

[2]Schuller, J. A., Barnard, E. S., Cai, W., Jun, Y. C., White, J. S., Brongersma, M. L., "Plasmonics for extreme light concentration and manipulation," *Nature Materials*, Vol. 9, No. 3, pp. 193-204, 2010.

[3]Yang, X., Liu, Y., Oulton, R. F., Yin, X., Zhang, X., "Optical Forces in Hybrid Plasmonic Waveguides," *Nano Letters*, Vol. 11, No. 2, pp. 321-328, Feb. 9, 2011.

[4]NASA, "2011 NASA Strategic Plan," http://www.nasa.gov/news/budget/index.html, 2011.

[5]Trauger, J., Stapelfeldt, K., Traub, W., Krist, J., Moody, D., Mawet, D., Serabyn, E., Henry, C., Brugarolas, P., Alexander, J., Gappinger, R., Dawson, O., Mireles, V., Park, P., Pueyo, L., Shaklan, S., Guyon, O., Kasdin, J., Vanderbei, R., Spergel, D., Belikov, R., Marcy,

G., Brown, R. A., Schneider, J., Woodgate, B., Egerman, R., Matthews, G., Elias, J., Conturie, Y., Vallone, P., Voyer, P., Polidan, R., Lillie, C., Spittler, C., Lee, D., Hejal, R., Bronowicki, A., Saldivar, N., Ealey, M., Price, T., "ACCESS: a concept study for the direct imaging and spectroscopy of exoplanetary systems," *SPIE Proceedings, Space Telescopes and Instrumentation 2010: Optical, Infrared, and Millimeter Wave*, Vol. 7731, pp. 773128-773128, August 06, 2010.

[6]Micci, M. M., Ketsdever, A. D., "Micropropulsion for Small Spacecraft," Progress in Aeronautics and Astronautics, Vol. 187, P. Zarchan, ed., American Institute of Aeronautics and Astronautics, Inc., Reston, VA, 2000.

[7]Meyer, M., Johnson, L., Palaszewski, B., Goebel, D., White, H., Coote, D., "NASA In-Space Propulsion Systems Roadmap: Technology Area 02," April 2012.

[8]Xu, H., Käll, M., "Surface-Plasmon-Enhanced Optical Forces in Silver Nanoaggregates," *Physical Review Letters*, Vol. 89, No. 24, pp. 246802, 2002.

[9]Wang, K., Schonbrun, E., Crozier, K. B., "Propulsion of Gold Nanoparticles with Surface Plasmon Polaritons: Evidence of Enhanced Optical Force from Near-Field Coupling between Gold Particle and Gold Film," *Nano Letters*, Vol. 9, No. 7, pp. 2623-2629, July 8, 2009.

[10]Miao, X., Wilson, B. K., Pun, S. H., Lin, L. Y., "Optical manipulation of micron/submicron sized particles and biomolecules through plasmonics," *Optics Express*, Vol. 16, No. 18, pp. 13517-13525, 2008.

[11]Pyatenko, A., Takeuchi, H., Chiba, S., Ohyama, Y., "Dispersion of fine powder agglomerates under microgravity," *AIChE Journal*, Vol. 47, No. 12, pp. 2696-2704, Dec. 2001.

[12]"NASA Space Technology Roadmaps and Priorities: Restoring NASA's Technological Edge and Paving the Way for a New Era in Space," Steering Committee for NASA Technology Roadmaps, National Research Council, 2012.

[13]de Vine, G., Ware, B., McKenzie, K., Spero, R. E., Klipstein, W. M., Shaddock, D. A., "Experimental Demonstration of Time-Delay Interferometry for the Laser Interferometer Space Antenna," *Physical Review Letters*, Vol. 104, No. 21, pp. 211103, 2010.

[14]Wertz, J. R., *Spacecraft attitude determination and control*, Reidel, Dordrecht; Boston, 1985.

[15]Liaw, D. C., Liu, T. M., Gilchrist, B. E., "Simulation of using background plasma to neutralize charged particle thrusters on nanospacecraft," *IEEE International Conference on Plasma Science (ICOPS)*, pp. 3P-26-3P-26, 8-13 July 2012.

[16]Thomas A. Moore. *Six Ideas That Shaped Physics, Unit N: The Laws of Physics are Universal*. McGraw-Hill, Second edition, 2003.

[17]Thomas A. Moore. *Six Ideas That Shaped Physics, Unit C: Conservation Laws Constrain Interactions*. McGraw-Hill, Second edition, 2003.

[18]George P Sutton, and Oscar Biblarz. *Rocket Propulsion Elements*. John Wiley & Sons, Inc., Eighth edition, 2010.

[19]Eugene Hecht. *Optics*. Addison-Wesley, Fourth edition, 2002.

[20]Th. Kwaaitaal. Contribution to the interferometric measurement of sub-angstrom vibrations. *AIP Review of Scientific Instruments*, 45(1):39-41, 1974.

[21]R.G. Klaver, and L.M. Krieg, and J.J.M. Braat. Measuring absolute optical path differences with angstrom accuracy over ranges of millimeters. *Proceedings Symposium IEEE/LEOS Benelux Chapter*, Delft, The Netherlands, 2000. Delft University of Technology.

[22]Meredith Gibb. LISA Laser Interferometer Space Antenna Project Office. http://lisa.nasa.gov/. Accessed: 2014-04-17.

[23]LISA: Study of the Laser Interferometer Space Antenna, Final Technical Report. *astrium*, 13631/99/NL/MS(LI-RP-DS-009), 2000.

[24]NASA, and esa. Laser Interferometer Space Antenna (LISA) Mission Concept. (LISA-PRJ-RP-0001), 2009.

[25]Thomas A. Moore. *Six Ideas That Shaped Physics, Unit Q: Particles Behave Like Waves*. McGraw-Hill, Second edition, 2003.

[26]Kenneth Carpenter. SI: The Stellar Imager. http://hires.gsfc.nasa.gov/si/. Accessed: 2014-04-17.

[27]Kenneth G. Carpenter *et. al*. SI-The Stellar Imager: A UV/Optical deep-space telescope to image stars and oberve the Universe with 0.1 milli-arcsec angular resolution. 2005.

[28]Jorgen Christensen-Dalsgaard, and Kenneth G Carpenter, and Carlus J Schrijver, and Margarita Karovska, and the SI Team. The Stellar Imager (SI) - A Mission to Resolve Stellar Surfaces, Interiors, and Magnetic Activity. *Journal of Physics: Confrence Series*, 271(012085), 2011.

[29]Marcel J. Sidi. *Spacecraft Dynamics and Control: A Practical Engineering Approach*. Cambridge University Press, Third edition, 1997.

[30]Peter Fortescue, and John Stark, and Graham Swinerd. *Spacecraft Systems Engineering*. Wiley, 2003.

[31]James R. Wertz. *Spacecraft Attitude Determination and Control*. Graphics Press, 1985.

[32]Wilam E. Wiesel. *Spaceflight Dynamics*. Aphelion Press, Third edition, 2010.

[33]J. A. Schuller, and E. S. Barnard, and W. Cai, and Y. C. Jun, and J. S. White, and M. L. Brongersma. Plasmon nano-optical tweezers. *Nature Photonics*, 5(6):349-356, 2011.

[34]M. L. Juan, and M. Righini, and R. Quidant. Plasmon nano-optical tweezers. *Nature Photonics*, 5(6):349-356, 2011.

[35]Wang, K., and Schonbrun, E., and Crozier, K. B.,. Propulsion of Gold Nanoparticles with Surface Plasmon Polaritons: Evidence of Enhanced Optical Force from Near-Field Coupling between Gold Particle and Gold Film. *Nano Letters*, 9(7):2623-2629, 2009.

[36]Yang, X., and Liu, Y., and Oulton, R. F., and Yin, X., and Zhang, X.,. Optical Forces in Hybrid Plasmonic Waveguides. *Nano Letters*, 11(2):321-328, 2011.

[37]Boris Lamontagne, and Py Christophe. Microblinds and a method of fabrication thereof. 2006.

[38]Alexey Shashurin, and Michael Keidar, and Taisen Zhuang. Comparative analysis of micro-cathode arc thruster performance. *33rd International electric Propulsion Conference*, Washington D.C., 2013. IEPC, Paper 2013-389.

[39]Taisen Zhuang, and Alexey Shashurin, and Isak Beilis, and Michael Keidar. Ion velocities in a micro-cathode arc thruster. *Physics of Plasmas*, 19(063501), 2012.

[40]Michael Keidar, and Samudra Haque, and Taisen Zhuang, and Alexey Shashurin, and Dereck Chiu, and George Teel. Micro-Cathode Arc Thruster for PhoneSat Propulsion. *27th Annual AIAA/USU Conference on Small Satellites*, Logan, Utah, 2013. Paper SSC13-VII-9.

[41]Taisen Zhuang, and Alexey Shashurin, and Samudra Haque and Michael Keidar. Performance characterization of the micro-Cathode Arc Thruster and propulsion system for space applications. *46th AIAA Joint Propulsion Conference and Exhibit*, Nashville, TN, 2010. AIAA 2010-7018.

[42]Alameda Applied Sciences Corporation. http://www.aasc.net/micropropulsion/vat/vat-specifications. Accessed: 2014-04-17.

[43]J. Schein, and N. Qi, and R. Binder, and M. Krishnan, and J. K. Ziemer, and J. E. Polk, and A. Anders. Inductive energy storage driven vacuum arc thruster. *Review of Scientific Instruments*, 73(2):925-927, 2002.

[44]Jochen Schein, and Niansheng Qi, and Robert Binder, and Mahadevan Krishahnan, and John Ziemer, and James Polk, and Andre Anders. Low Mass Vacuum Arc Thruster System for Station Keeping Missions. *IEPC-01-228*, Pasadena, CA, 2001. International Electric Propulsion Confrence.

[45]Tamer Akan, and Serdar Demirkol, and Naci Ekem, and Suat Pat, and Geavit Musa. Study of Metal and Ceramic Thermionic Vacuum arc Discharges. *Plasma Science and Technology*, 9(3):280-283.

[46]Clyde Space and Mars Space LTD. http://www.clyde-space.com/cubesat_shop/propulsion/303_cubesat-pulse-plasma-thruster. Accessed: 2013-11-18.

[47]Tom Roy, and Vlad Hruby, and Nathan Rosenblad, and Peter Rostler, and Douglas Spence. CubeSat Propulsion Using Electrospray Thrusters. *23rd Annual AIAA/USU Conference on Small Satellites*, 2009. SSC09-II-6.

[48]F. Martel, and P. Lozano. Ion Electrospray thruster Assemblies for CubeSats. *iCubeSat Workshop*, Cambridge, 2012. Massachusetts Institute of Technology.

[49]J. Mueller, and J. Ziemer, and R. Hofer, and R. Wirz, and T. O. Donnell. A Survey of Micro-Thrust Propulsion Options for Microspacecraft and Formation Flying Missions. *CubeSat 5th Annual Developers Workshop*, San Luis Obispo, CA, 2008. California Polytechnic State University.

[50]L. F. Velasquez-Garcia, and A. I. Akinwande, and M. Martinez-Sanchez. A Planar Array of Micro-Fabricated Electrospray Emitters for Thruster Applications. *Journal of Microelectromechanical Systems*, 15(5):1272-1280, 2006.

[51]Blue Canyon Technologies. www.bluecanyontech.com. Accessed: 2014-04-17.

[52]C.L. Cheung, and R.J. Nikolic, and C.E. Reinhardt, and T.F. Wang. Fabrication of nanopillars by nanosphere lithography. *Nanotechnology*, 17(5):1339-1343, 2006.

[53]John C. Hulteen, and Richard P. Van Duyne. Nanosphere lithography: A materials general fabrication process for periodic particle array surfaces. *American Vacuum Society*, 13(3):1553-1558, 1995.

[54]Wei Wu, and Dibyendu Dey, and Omer G. Memis, and Alex Katsnelson, and Hooman Mohseni. Fabrication of Large Area Periodic Nanostructures Using Nanosphere Photolighography. *Nanoscale Res Lett*, 3:351-354, 2008.

[55]Richard C. Dorf, and Robert H. Bishop. *Modern Control Systems*. Prentice Hall, Ninth edition, 2000.

[56]M. Coletti, and F. Guarducci, and S. B. Gabriel. A micro PPT for Cubesat application: Design and preliminary experimental results. *Elsevier*, 69:200-208, 2011.